

# Average UV Quasar Spectra in the Context of Eigenvector 1: A Baldwin Effect Governed by Eddington Ratio?

R. Bachev<sup>1,2</sup>, P. Marziani<sup>3</sup>, J. W. Sulentic<sup>1</sup>, R. Zamanov<sup>3,4</sup>, M. Calvani<sup>3</sup>, D. Dultzin-Hacyan<sup>5</sup>

## ABSTRACT

We present composite UV spectra for low redshift Type 1 AGN binned to exploit the information content of the Eigenvector 1 (E1) parameter space. Composite spectra show high enough S/N and spectral resolution to permit a decomposition of the CIV $\lambda$ 1549 line profile – one of the strongest high-ionization lines (HIL) and fundamental in defining E1 space. The simplest CIV $\lambda$ 1549 decomposition into narrow (NLR), broad (BLR) and very broad (VBLR) components suggests that different components have an analog in H $\beta$  with two major exceptions. VBLR emission is seen *only* in population B (FWHM(H $\beta$ <sub>BC</sub>)>4000 km s<sup>-1</sup>) sources. A blue shifted/asymmetric BLR component is seen *only* in population A (FWHM(H $\beta$ <sub>BC</sub>) $\leq$ 4000 km s<sup>-1</sup>) HIL such as CIV $\lambda$ 1549. The blueshifted component is thought to arise in a high ionization wind or outflow. Our analysis suggests that such a wind can only be produced in population A (almost all radio-quiet) sources where the accretion rate is relatively high. We propose a model to account for several differences between low- and high-ionization line profiles. Part of the broad line emission is attributed to a self-gravitating/fragmented region in an accretion disk. An inner optically thick geometrically thin region of the flow may give rise to a wind/outflow and produce the blueshifted HIL spectrum

---

<sup>1</sup>Department of Physics and Astronomy, University of Alabama, Tuscaloosa, AL 35487, USA; giacomomo@merlot.astr.ua.edu

<sup>2</sup>Institute of Astronomy, Sofia 1784, Bulgaria; bachevr@astro.bas.bg

<sup>3</sup>INAF, Osservatorio Astronomico di Padova, Vicolo dell'Osservatorio 5, I-35122 Padova, Italy; marziani@pd.astro.it; calvani@pd.astro.it

<sup>4</sup>National Astronomical Observatory Rozhen, POB 136, Smoljan, BG-4700, Bulgaria

<sup>5</sup>Instituto de Astronomía, UNAM, Apdo. Postal 70-264, 04510 Mexico D.F., Mexico; debo-rah@astroscu.unam.mx

in Pop. A sources. The fragmented region may produce all or most of the broad line emission in population B, which contains radio-quiet and the majority of radio-loud quasars. Comparison between *broad* UV lines in radio-loud (RL) and radio-quiet (RQ) sources in a single well populated E1 parameter space bin (B1) shows few significant differences. Clear evidence is found for a significant NLR CIV component in most radio-loud sources. The BLR/VBLR similarity in bin B1 provides circumstantial evidence in favor of black hole (BH) spin, rather than BH mass or accretion rate, as a key trigger in determining whether an object will be RL or RQ. We find a ten-fold decrease in EW CIV $\lambda$ 1549 with Eddington ratio (decreasing from  $\approx 1$  to  $\sim 0.01$ ) while Nv $\lambda$ 1240 shows no change. These trends suggest a luminosity-independent "Baldwin effect" where the physical driver may be the Eddington ratio.

*Subject headings:* quasars: emission lines – quasars: general

## 1. Introduction

Understanding the geometry and kinematics of the central regions in AGN is one of the major goals of twenty-first century astronomy. Yet little is known beyond the necessity of invoking accretion onto a supermassive object in order to account for the enormous source luminosity. Given our inability to resolve the central regions of even the nearest AGN we are left with three approaches towards achieving our goal: (1) ideology: sophisticated models driven entirely by theories describing black hole and associated accretion disk properties (e.g., Janiuk, Życki, & Czerny 2000; Gammie, Shapiro, & McKinney 2004), (2) analogy: comparison with better-resolved galactic objects (e.g. interacting binary stars; Zamanov & Marziani 2002; Mirabel 2004; Maccarone, Gallo, & Fender 2003) and (3) empiricism: detailed studies of phenomenology in large and diverse samples of AGN (see Sulentic, Marziani & Dultzin-Hacyan 2000a for references until late 1999; Marziani et al. 2003a, hereafter M03; Dietrich et al. 2002; Kuraszekiewicz et al. 2004 for examples of more recent works). The last approach fell on hard times until the end of the twentieth century in part due to: (i) the apparent intractability of AGN phenomenology, (ii) the failure of the best nebular physics models to reproduce the observed spectra, and (iii) the low quality of so much of the spectroscopic data. Thus we now know more about the morphology of the extended radio and optical emission around quasars than the underlying geometry/physics that drives them. One positive development involves the application of reverberation mapping towards estimation of the broad line region size (see Peterson 1993 for a thorough review; Horne et al., 2004 for up-to-date expectations). The relevant questions are how to interpret these data

and, more importantly, how to select a representative sample of sources for a reverberation mapping study. Another positive development involves growing databases of AGN spectra (most notably from the Sloan Digital Sky Survey (SDSS); Richards et al. 2002; Schneider et al. 2002). Although great part of the individual data still suffers from S/N limitations, average or composite spectra of many objects can significantly improve the situation (Vanden Berk et al. 2001; Sulentic et al. 2002). One of the most important questions is *how* to bin the data. Clearly unrestricted composites have little value because they hide the intrinsic dispersion in key parameters which provides clues to the underlying physics (e.g., Francis et al. 1991). In a previous paper (Sulentic et al. 2002: hereafter Paper I) we argue that composite spectra binned within the Eigenvector 1 parameter space provide the most physically useful results. Paper I presented composites of the  $H\beta$  spectral region and this paper presents complementary composites for the UV spectral region and especially for  $CIV\lambda 1549$ .

We have identified a four dimensional parameter space that overcomes some of the problems mentioned above and that offers a new perspective on AGN phenomenology (Sulentic et al. 2000a,b). The Eigenvector 1 (E1) parameter space provides optimal discrimination/unification of broad-line AGN classes (Boroson & Green 1992; Marziani et al. 2001, hereafter M01; Boroson 2002). The adopted name reflects recognition of the first two parameters in the pioneering work of Boroson & Green (1992). E1 as we now define it involves measures of:

1. full width at half maximum of low ionization (LIL) broad emission lines  $[FWHM(H\beta_{BC})]$ ,
2. equivalent width ratio of optical FeII and  $H\beta_{BC}$ :  $R_{FeII}=EW(FeII \lambda 4570 \text{ blend})/EW(H\beta_{BC})$ ,
3. soft X-ray photon index ( $\Gamma_{\text{soft}}$ ),
4. profile centroid velocity displacement (at FWHM) for  $CIV\lambda 1549$ .

In simplest terms these parameters can be said to measure respectively: (1) velocity dispersion of LIL emitting gas, (2) relative strength of LIL features thought to arise in the same region, (3) strength of a soft X-ray component and (4) amplitude of systematic motions in the high-ionization line (HIL) emitting gas. In less simple (i.e. more model dependent) terms we likely have: (i) two variables mainly sensitive to accretion rate ( $FWHM(H\beta_{BC})$  and  $\Gamma_S$ : Nicastro 2000; M01; Pounds, Done & Osborne 1995; Czerny et al. 2004), (ii) three variables sensitive to source orientation (all with the possible exclusion of  $\Gamma_S$ ; e.g., Jackson & Browne 1991; Wills et al. 1995; Marziani et al. 1996; M01; Rokaki et al. 2003; Sulentic et al. 2003).  $R_{FeII}$  is sensitive to nebular physics (electron density  $n_e$  and column density  $N_c$ ).

An important addition that reflects the striking changes in emission line properties across E1 involves introduction of the population A and B concept. At present we arbitrarily define Pop. A and B quasars as those with FWHM  $H\beta_{BC}$  less than or greater than  $4000 \text{ km s}^{-1}$ . It is unclear whether the A-B concept reflects two distinct quasar populations or simply the difference in mean properties of sources at opposite ends of the E1 "main sequence". The "elbow" shape of the sequence, and optical/X-ray indications (Sulentic et al. 2000a,b; Komossa & Meerschweinchen 2000) for a "zone of avoidance" near  $\text{FWHM}(H\beta_{BC}) \approx 4000 \text{ km s}^{-1}$ , provide some evidence in support of the former interpretation. If the distinction is real then "A" is a largely RQ population (including narrow line Seyfert 1 sources as an extremum), while "B" contains a mix of broader line RQ plus most RL sources. The population A-B distinction will prove useful in this study and  $\text{CIV}\lambda 1549$  will add support for the concept (§3.2 and §4.3).

If the E1 concept lives up to initial promise, it may be the strongest and most encompassing type-1 AGN unification yet discovered. This possibility warrants strong tests of its strength and generality. So far most of our effort has centered on the "optical plane" of E1 (M01; Zamanov et al. 2002; Boroson 2002; Marziani et al. 2003a,b; Sulentic et al. 2003). This focus has been dictated by the available X-ray and UV archival data that provide the other E1 parameters. In the next section we present composite spectra for  $\text{CIV}\lambda 1549$  (and other UV lines) in the E1 context which complements work already done for  $H\beta$ .

## 2. Generating Composite UV Spectra

A total of about 700 reasonable quality ( $S/N^1 \geq 4-5$ ) HST spectra for  $n = 141$  different AGN (quasars or bright Seyfert 1's;  $n=61$  are radio-loud with  $R_K \gtrsim 100$ , where  $R_K$  is the specific flux ratio between  $4400 \text{ \AA}$  and  $6 \text{ cm}$ ) have been extracted from the Hubble archive. The majority of the spectra (83 %) were obtained with the FOS camera and the rest with STIS. The FOS/BL data (40 %) were recalibrated with the latest IRAF package – STPOA, which takes into account some systematic errors in the wavelength calibration. No such recalibration is available for the FOS/RD, where similar errors are known to exist, which ultimately limits the wavelength accuracy of our composites to about  $0.5-1.0 \text{ \AA}$  (see for instance Kerber & Rosa, 2000, for details on FOS calibration).

Composite spectra cover the entire rest frame region between  $1000-3000 \text{ \AA}$  while individual source spectra will often cover only a part of it. We applied the following procedures

---

<sup>1</sup>Here and below  $S/N$  is the signal-to-noise ratio per resolution element, measured in the continuum, blueward of  $\text{CIV}\lambda 1549$

to compute the composite spectra:

1. Spectra for a specific source covering the same spectral region were averaged together (if they were of comparable S/N).
2. A single spectrum for each object was created by adding the parts covering different wavelength regions, with slight adjustments of the continuum levels if necessary.
3. All spectra were corrected for Galactic extinction following Schlegel et al. (1998). The typical extinction correction  $A_V$  was about 0.1 – 0.2 magnitude. No correction for the intrinsic extinction was attempted.
4. The spectra were de-redshifted using the most accurate available measurements (M03) or by using the latest accurate values available in the literature whenever a source was not part of the M03 sample<sup>2</sup>. It should be noted that redshifts from Véron-Cetty & Véron (2001); hereafter VCV01, sometimes differ considerably from our best values ( $\Delta z$  could be as large as 0.02).
5. Spectra were normalized by their own continuum flux in the wavelength range 1430–1470 Å, where no strong lines are observed/expected.
6. Composite spectra were generated by median-combining the averaged spectra of individual AGN. This procedure ensures that only the most typical features will be revealed, and that some unusual features like narrow absorption (often lost in the noise), unusually strong (narrow) lines, noise spikes, etc. will be omitted in the composites. A median also works better than an average when the individual spectra do not cover the same spectral region (see §4 for details regarding line profiles of the composites).

The composites have been binned to 0.5 Å per resolution element and have a typical S/N~50 (see Table 1). The composite spectra are presented in Figure 1 with an enlargement of the 1100–2000 Å region of greatest interest shown in Figure 2. The latter show details of the strongest lines such as Ly $\alpha$ , CIV $\lambda$ 1549, and CIII] $\lambda$ 1909. The lines that we identified and measured (§3.1) are labeled.

We defined spectral types on the basis of source parameter properties in the optical plane of E1 (Paper I). This approach differs from the one employed in analysis of the SDSS quasar sample (Richards et al. 2002) where sources were binned *a posteriori* in terms of the

---

<sup>2</sup>M03 did not publish most of their refined redshift measures based on [OIII] $\lambda$ 5007 or the narrow peak of H $\beta$  (see Zamanov et al. 2002); they are available from the authors on request.

velocity shift between CIV $\lambda$ 1549 and MgII $\lambda$ 2800. We are able to create useful composites for five E1 bins with fixed FWHM(H $\beta$ <sub>BC</sub>) and R<sub>FeII</sub> ranges, exactly as done in Paper I. The values of FWHM(H $\beta$ <sub>BC</sub>) and R<sub>FeII</sub> that provide an optical bin assignment were taken from M03. In order to maximize the number of sources in each bin we also include additional spectra for sources ( $\approx 20\%$  of the total), not part of the M03 sample. This supplemental data involves: 1) sources with reasonable quality archival CIV $\lambda$ 1549 data and 2) H $\beta$  spectra from literature sources with high enough S/N to permit assignment into one of the predefined E1 bins. Details on bin assignment for individual sources that are not part of the M03 sample will be provided in a future work.

Table 1 provides parameter measures and statistical properties for the spectral bins. The format is: Column 1 – spectral type designation following Paper I; Col. 2 – range of FWHM(H $\beta$ <sub>BC</sub>); Col. 3 – range of R<sub>FeII</sub>; Col. 4 – number of sources used for the composite spectrum (number of RL source in parenthesis). Each bin typically involves 15 – 30 sources resulting in a S/N in the continuum typically of 40 – 60 (Col. 5). Col. 6 and 7 present the average absolute  $V$ -magnitude (computed from VCV01;  $H_0 = 50 \text{ km s}^{-1} \text{ Mpc}^{-1}$ ;  $q_0 = 0$  is adopted) and redshift for sources used in the bin composite followed by the sample standard deviations. We also present the average equivalent widths (EW) of [OIII] $\lambda$ 5007 and H $\beta$  for the objects of the sample – Col. 8 and 9 respectively.

There is a clear trend between  $\langle M_V \rangle$  and  $z$ , in the sense that Pop. A sources show lower mean redshift and luminosity. This is a known bias in the M03 dataset. M03 is a step towards our goal to develop a sample complete to  $m_V=16.5$ . At this time the radio-loud part of our sample is apparently complete (the standard  $V/V_{\text{max}}$  completeness test (e.g., Peterson 1997) gives  $\sim 0.8$  compared to 0.3 for RQ sources). The radio loud sources tend to be more luminous (due in part to relativistic beaming) resulting in selecting more high redshift sources. The E1 optical parameters *show no dependence on luminosity* to at least  $z \lesssim 1$  and  $m_V \lesssim 16.5$  (Sulentic et al. 2004). We will consider later possible UV line vs. source luminosity correlations (see §3.3 and §4.3).

We also computed the sample standard deviation for the spectra in each bin. Deviations from the composites at  $1\sigma$  confidence level are found to be about 20% and show no specific features after being normalized by the composites themselves.

### 3. UV Lines in the E1 Context

#### 3.1. FeII<sub>UV</sub> subtraction and line measurements

Table 2 presents rest-frame EW and FWHM measures for UV lines in the composite spectra. E1 bin designations are listed at the top of the Table. Uncertainty estimates are given in parenthesis following each measure. EW uncertainties are about 10–20% for the strongest lines ( $W \gtrsim 10 \text{ \AA}$ ) and approach 50% for the weaker lines. FWHM uncertainties are generally below 20–30% with the level of uncertainty depending on S/N of the composites as well as line blending (e.g. Si IV $\lambda$ 1398) in some cases. All measurements were carried out after FeII<sub>UV</sub> and continuum subtraction except that these corrections were not applied to MgII $\lambda$ 2800.

The FeII<sub>UV</sub> template covering the 1000 – 2000  $\text{\AA}$  region (where the most interesting lines are) was created with spectra for I Zw 1 (see Marziani et al. 1996, M03 for details). The template was intensity scaled and broadened in order to best match the observed FeII pattern in the composite spectra. The results are summarized in the last row of Table 2. Figure 3 illustrates the deblending results for two particularly important groups of lines: Ly $\alpha$  + Nv $\lambda$ 1240 and Al III $\lambda$ 1860 + Si III] $\lambda$ 1892 + CIII] $\lambda$ 1909. The first blend is important because Nv $\lambda$ 1240 is the only high-ionization line that shows no significant Baldwin effect (Sulentic et al. 2000a, see also §4.5). The importance of the second blend involves the fact that the intensity ratio Si III] $\lambda$ 1892/ CIII] $\lambda$ 1909 may be sensitive to density ( $n_e$ ) and/or may be affected by metallicity trends along E1 (M01; §4.3). We carried out a deblending procedure by assuming a Lorentzian profile for both lines in the blend and allowing for different component intensities and FWHM. A possible contamination by FeIII blends may contribute to some extent to the relatively poor fit of these lines in A3 bin.

We consider several interesting results that can be summarized as follows:

- OVI $\lambda$ 1034, Ly $\alpha$ , CIV $\lambda$ 1549, CIII] $\lambda$ 1909 and MgII $\lambda$ 2800 show a systematic increase in equivalent width as one proceeds from extreme population A (bin A3) towards the B bins. The most dramatic change is actually seen in MgII $\lambda$ 2800, CIV $\lambda$ 1549 and also OVI $\lambda$ 1034, where bin averaged equivalent widths increase by almost a factor of four (a factor  $\sim 10$  is seen in CIV $\lambda$ 1549 if individual sources are considered). While we adopted CIV centroid shift at FWHM as an E1 parameter other CIV measures follow the E1 sequence as well.
- Contrary to the above lines Nv $\lambda$ 1240 shows almost constant equivalent width ( $\approx 20 - 25 \text{ \AA}$ ) across the E1 sequence. Other lines show no clear trends within measurement uncertainties.

- The Si III] $\lambda$ 1892/ C III] $\lambda$ 1909 intensity ratio decreases monotonically by a factor of four as one proceeds from bin A3 to B1<sup>+</sup> (from 0.8 to 0.2). See §4 for possible explanations.
- We find a clear positive trend between FWHM and ionization potential ( $\chi$ ) for the principal broad lines. The correlation coefficients are in the range 0.6–0.8. FWHM typically scales linearly with  $\chi$  up to  $\chi \lesssim 50$  eV and saturates beyond that value. The scatter in this relation appears to be smaller for A-bins. B-bins suggest that some LIL such as Mg II  $\lambda$ 2800 and Ly $\alpha$  deviate from the relationship with larger than expected values of FWHM. The linear part of the relation can be roughly described by the following expression:  $FWHM = V_0 + \alpha\chi$ , where  $\alpha \sim 60 - 80$  and  $V_0$  from 1000 to 3000 km s<sup>-1</sup> from bin A3 to B1<sup>+</sup>. The saturation occurs at about 4000 km s<sup>-1</sup> for A-bins and at about 5000 – 6000 km s<sup>-1</sup> for B-bins.

### 3.2. CIV $\lambda$ 1549 Profile Decomposition

The CIV $\lambda$ 1549 line deserves special attention as the best studied, and easiest to study, HIL. The CIV $\lambda$ 1549 intensity and relative lack of contamination by satellite lines, motivated its selection as the representative HIL in the E1 parameter space. Profile centroid shift at FWHM intensity was chosen as one of the most important E1 parameters (Sulentic et al. 2000b). The blueshifted component of the CIV $\lambda$ 1549 line seems to disappear in sources with FWHM  $H\beta_{BC} \geq 4000$  km s<sup>-1</sup> providing further support for the pop. A-B distinction. This fact and other previous works make it clear that both HIL and LIL cannot be treated as single component lines. A large part of the confusion in past broad line studies stems from this fact. The simplest possible decomposition of our composite CIV $\lambda$ 1549 profiles was attempted after the following processing steps. 1) The continuum was subtracted by fitting a low-order Lagrange polynomial over the region 1000–2000Å. 2) A broadened and scaled Fe II<sub>UV</sub> template was subtracted (§3.1, Table 2). Fe II<sub>UV</sub> emission is not strong in any of the bin composites however a reasonable correspondence between the optical and UV Fe II emission strengths can be traced in the sense that bin A3 shows the strongest Fe II<sub>UV</sub> emission. 3) Contaminating lines near CIV $\lambda$ 1549: N IV] $\lambda$ 1486 and blended He II  $\lambda$ 1640 + O III] $\lambda$ 1663 were fitted with Lorentzians and subtracted from the CIV $\lambda$ 1549 wings. 4) A narrow component was subtracted from the CIV $\lambda$ 1549 profile (see below).

Results of the CIV $\lambda$ 1549 decomposition are given in Figure 4 and Table 3. Results from modelling our  $H\beta_{BC}$  composites (Paper I) are useful here. We identified three reasonably unambiguous  $H\beta$  components in the context of E1 and the Population A-B hypothesis. These identifications, and the adopted profile fits, are largely empirical at this stage. We focus on bins A2/A3 and B1 as representative of the two AGN populations or E1 parameter



space extrema. Bin A1 is likely a mix of both population A and B sources (or a transition between the two).

- **i) NLR**

**H $\beta$ :** We often see an inflection between the BLR and NLR components of LIL H $\beta$  making profile decomposition less ambiguous (Marziani et al, 1996). Bins A2/A3 show evidence for weak H $\beta_{\text{NC}}$  emission ( $EW \simeq 3 \text{ \AA}$ ) in residuals after modelling the broad line components (Paper I). A more significant NLR component is found in the majority of Pop B sources ( $EW > \simeq 5 - 6 \text{ \AA}$  with a large scatter). If we assume a fixed ratio for H $\beta_{\text{NC}}/[\text{OIII}]\lambda 5007$ , then the Table 1 averages for EW( $[\text{OIII}]\lambda 5007$ ) imply a very weak H $\beta_{\text{NC}}$  contribution in bins A2/A3. This ratio is about 0.11 for pop. B sources which would imply  $EW(\text{H}\beta_{\text{NC}}) \simeq 1 \text{ \AA}$  for bins A2/A3 which is lower than what we actually subtracted except in the "blue outlier" sources where  $[\text{OIII}]\lambda 5007$  is extremely weak and blueshifted (Zamanov et al. 2002).

**CIV $\lambda 1549$ :** In our opinion it is clear that a narrow CIV $\lambda 1549_{\text{NC}}$  component exists in many, especially Pop. B, sources because we can see a profile inflection (Sulentic & Marziani 1999). The situation for CIV $\lambda 1549$  is more ambiguous than for H $\beta_{\text{BC}}$  because of the lower intrinsic resolution (and often S/N) of the CIV $\lambda 1549$  spectra which less often show the inflection that can guide a profile decomposition. Either Gaussian or Lorentzian fits to the broad CIV $\lambda 1549$  profiles of bin A1, B1 and B1<sup>+</sup> composites show a narrow residual. Although one cannot be sure that it is from an NLR component, that is the simplest interpretation and is empirically justified by many cases where NLR emission is unambiguously observed. New evidence for an NLR component in, at least, pop B RL quasars is given in §4.4. We therefore argue that an uncertain NLR subtraction is better than no subtraction for the A1 and B-bins. No NLR component was subtracted from bins A2/A3. The NLR profile width was assumed  $\text{FWHM} \lesssim 2000 \text{ km s}^{-1}$  (taking into account the fact that CIV $\lambda 1549$  is a doublet). Photoionization models suggest  $EW(\text{CIV}\lambda 1549_{\text{NC}}) \simeq 0.1 \text{ EW}([\text{OIII}]\lambda 5007)$  as a reasonable estimate (i.e. about 2 – 4  $\text{\AA}$ , using the EW( $[\text{OIII}]\lambda 5007$ ) values from Table 1 and Paper I). We should point out that this EW ratio is rather similar to the flux ratio of the lines since the continuum shape does not seem to change significantly along the E1 bins (Fig. 1). Without inter-calibration of optical and UV fluxes, as well as knowledge of the NLR extinction properties (e.g. Netzer & Laor 1993), such numbers are only indicative. See Sulentic & Marziani (1999) for more quantitative estimates of the effect of a CIV $\lambda 1549$  NLR component on measures of FWHM and line shift. Our adopted estimates of  $EW(\text{CIV}\lambda 1549_{\text{NC}})/EW(\text{CIV}\lambda 1549_{\text{BC}})$  show a large scatter (0.0 – 0.5) among individual sources in A1 and B-bins.

• ii) BLR

$H\beta$ : This is the defining broad-line component for Type 1 AGN. The Population A–B distinction is currently defined in terms of sources with FWHM  $H\beta_{BC}$  smaller or larger than  $4000 \text{ km s}^{-1}$ . Pop. A2/A3 bin composites are best fit by an unshifted Lorentzian function (Véron-Cetty et al. 2001) while for Pop B bins a Gaussian model works better. While the bin composite profiles are unshifted, individual sources can show red or blue shifts of up to  $4000 \text{ km s}^{-1}$ . Profile shifts larger than about  $600 \text{ km s}^{-1}$  are seen only in Pop. B sources (Sulentic et al. 2000a,b). Double peaked profiles are also sometimes ( $\leq 5\%$ ) seen in bins B1<sup>+</sup> and B1<sup>++</sup> <sup>3</sup>. Measures of FWHM  $H\beta_{BC}$  can be strongly influenced by the NLR component (e.g.  $L/L_{Edd}$  and BH mass over- and under-estimated, respectively).

**CIV $\lambda$ 1549**: A strongly blueshifted line or line component is seen only in Population A sources. The red half of the bin A2/A3 composite profiles can be reasonably well fit with an unshifted Lorentzian model whose strength is inferred from the amount of flux redward of the adopted source rest frame. In this context extreme A3 sources should have only a weak unshifted component with the bulk of the line flux strongly blueshifted. We don’t know if this decomposition has any physical meaning, i.e. whether we have two distinct line emitting regions or a single region, producing a complex profile. There are two admittedly empirical reasons to favor the two-component model:

1.  $H\beta_{BC}$  is best fit with an unshifted Lorentzian and there is no *a priori* physical reason why some HIL emission could not be produced in the clouds responsible for the LIL emission. Current models do not rule out the possibility of significant CIV emission from the LIL clouds (Korista et al., 1997), although the accurate quantitative predictions require extensive knowledge of the physical conditions there. The derived width of the best fit CIV $\lambda$ 1549 Lorentzian components are in good agreement with those estimated for  $H\beta_{BC}$  (about  $2500 \text{ km s}^{-1}$ , see Paper I).
2. The fits in Figure 4 are consistent with a systematically increasing unshifted component as one proceeds from Bin A3 to B1. The blueshifted (bulk of the emission in bins A2/A3) would be strongly blue asymmetric and would truncate rather sharply near the rest frame velocity, an interesting challenge for physical models. This truncation is actually seen in sources like I Zw1 and Ton 28 where a single component model is more appropriate (Sulentic et al. 2000b, 2001). We cannot distinguish between a Gaussian or Lorentzian model for the Pop. B BLR. The choice will affect our estimate of the

---

<sup>3</sup>Bin B1<sup>++</sup> was defined in Paper I for sources with  $R_{FeII} < 0.5$  and  $8000 \text{ km s}^{-1} \lesssim \text{FWHM}(H\beta_{BC}) \lesssim 12000 \text{ km s}^{-1}$

strength of the underlying VBLR. Results from  $H\beta_{BC}$  fits lead us to favor, by analogy, a two Gaussian model for  $CIV\lambda 1549$  Pop. A sources involving unshifted BLR plus redshifted VBLR components. At this point we cannot place much physical meaning on these Lorentzian vs. Gaussian fits, they simply reflect the relative sharpness of the line peak and the extent of the profile wings.

- **iii) VBLR**

$H\beta$ : There is no consensus whether or not the VBLR is a distinct component (e.g. Corbin 1997; Snedden & Gaskell, 2004; Korista & Goad 2004). Only Pop B sources appear to show this "red shelf" or component that we model as a separate VBLR (see references in Sulentic et al. 2000a). We prefer to speak of the VBLR as a distinct component for at least two reasons: 1) we often see an inflection between the red wing of the best fit BLR Gaussian and the red feature and 2) we have identified sources that only show a VBLR component (Sulentic et al. 2000c). Paper I composites suggest that the best current description of the components involve: i) a BLR with zero mean shift and  $FWHM \sim 5000 - 6000 \text{ km s}^{-1}$  as well as 2) a VBLR with mean redshift of about  $5000 \text{ km s}^{-1}$  and  $FWHM \simeq 10000 \text{ km s}^{-1}$ .

$CIV\lambda 1549$ : No evidence for a significant VBLR component is seen in population A bins paralleling the results for  $H\beta_{BC}$ . A double Gaussian decomposition is consistent with both BLR and VBLR  $CIV\lambda 1549$  components in Pop B bins<sup>4</sup>.  $FWHM$  of the components are in rough agreement with those for  $H\beta$ . Interestingly  $CIV\lambda 1549$  VBLR line shifts appear to be lower ( $\sim 1000 \text{ km s}^{-1}$ ) than those modeled in the  $H\beta_{BC}$  composites, however this may be a result of the fact that the two-component fitting is not necessarily a unique operation.

Furthermore line shift values derived for such an ultra-broad component must be considered very uncertain especially given the low S/N of many HST spectra.

While we currently separate population A and B sources at  $FWHM(H\beta_{BC}) = 4000 \text{ km s}^{-1}$ , if the distinction has any meaning then it will likely involve a complex combination of parameters. There are two possible interpretations of the Pop. A-B concept: i) two distinct AGN populations with different central source geometry and kinematics involving perhaps a critical Eddington ratio or ii) a single "main sequence" involving the majority of AGN and driven by a gradual change in the ionization parameter/Eddington ratio (see

---

<sup>4</sup>Although we fit A1 profile with a single Lorentzian, we cannot rule out the possibility that (some) A1 sources have both – a weak VBLR and a weak blue-shifted (wind) component, which along with a central unshifted component mimic a single Lorentzian.

M01). The "elbow" shape of the source occupation in the optical plane of E1 is an argument in favor of the former interpretation (i.e. it is not a monotonic correlation). In any case the shape suggests that bin A1 will likely blend the parameter space properties of Pop. A and B sources. Figure 4 and Tables 1, 2 support that view. A few sources in bin A1 (e.g. NGC 1566 and Mrk 493) show very strong NLR emission while others little or none. Our CIV $\lambda$ 1549 profile analysis supports the Population A-B idea in the sense that we find CIV $\lambda$ 1549 line components unique to each (Pop. A – blueshifted BLR, and Pop B – redshifted VBLR) but mutually exclusive.

Our results appear to be robust for sources with  $z < 0.8$ . Richards et al. (2002) created similar CIV $\lambda$ 1549 composite spectra using part of the much larger and higher mean redshift ( $\langle z \rangle \simeq 1.8$ ) SDSS quasar sample. Their spectral resolution is similar to our own but the S/N of individual spectra are usually much lower. They binned spectra showing CIV $\lambda$ 1549 into four groups (each involving almost 200 sources) based on the centroid shift of CIV $\lambda$ 1549. We lack LIL data that would allow us to assign unambiguous population A and B tags to these bins but the two extreme groups (Richards et al. composite D: most blueshifted and composite A: least shifted) should, more or less, correspond to our A2/A3 and B1/B2 samples respectively. If this statement is true then E1 predicts SDSS composite A sample should contain many radio-loud sources and composite D very few. We also note that SDSS composite A is more sharply peaked than composite D, consistent with a stronger NLR component. We applied our profile decomposition procedure to the SDSS A and D composites kindly provided by G. Richards and the results quantitatively verify the previous statement about their similarity to our lower redshift composites. The profiles are also consistent with the presence of a growing (from D to A) unshifted BLR component that further supports our two component fits to the bin A2/A3 composites. Richards et al. (2002) interpret the overall shift of CIV $\lambda$ 1549 as the result of "missing" flux on the red side of the profile. We think that the body of evidence, within the E1 context, does not support this interpretation, e.g. the blue wing of CIV $\lambda$ 1549 in extreme pop. A sources does not resemble the blue wing of CIV $\lambda$ 1549 in the broader pop. B sources. Similarly the blue wing on SDSS composite D is steeper than that for composite A. If we relate missing flux to obscuration then it would be surprising to find the strongest soft X-ray emission from sources with the most extreme blueshifted CIV $\lambda$ 1549 profiles since both should hardly be related.

SDSS composites cannot be used to help us decide whether there is a continuous "main sequence" in E1 or two distinct populations. Caution is needed in interpreting the SDSS binning because we do not know what the SDSS bin definition means in an E1 context, especially when MgII $\lambda$ 2800 (wings) may be strongly affected by FeII emission. If MgII $\lambda$ 2800 follows the line shift behavior of H $\beta$ <sub>BC</sub> large relative shifts CIV $\lambda$ 1549 – MgII $\lambda$ 2800 can occur

in pop. A because of CIV $\lambda$ 1549 blueshifts and in pop. B because of possible MgII $\lambda$ 2800 redshifts. If CIV $\lambda$ 1549 blueshifts (relative to rest frame and not MgII $\lambda$ 2800) remain a population A phenomenon at high redshift then the SDSS results suggest that the fraction of population A sources is larger at high redshift (75% vs. our estimate that 60% of quasars are population A; Marziani et al. 2003b). This would be consistent with our suggestion that Pop. A sources represent the "seed" population of young quasars in the Universe (Sulentic et al. 2000a; Mathur, 2000; Constantin & Shields, 2003).

### 3.3. RL – RQ Differences and Luminosity Effects

We can also compare RL vs. RQ properties using suitably constructed composites. Selection of RQ and RL subsamples from a single bin will ensure that we compare quasars with similar physical and observational properties. An extreme comparison of Pop. A vs. B will not be possible using a single bin. We would have to compare an extreme pop. A bin with an extreme pop. B one. Instead this will be a comparison between RL sources and RQ sources with optical spectra indistinguishable from them. This comparison offers hope to isolate subtle effects that might be direct manifestations of radio loud activity. We must use a B bin for this comparison because that is where most RL sources are found. We choose B1 which is the most densely populated and where RL and RQ objects are almost evenly represented. Radio (6cm) and optical V-band fluxes were derived from data in the VCV01 catalog. A radio-index (Kellermann et al. 1989)  $R_K$  was computed and all sources with  $\log(R_K) > 2$  are considered radio-loud (see Sulentic et al. 2003). Figure 5 shows the RL and RQ composites, as well as RL–RQ residuals, for both Ly $\alpha$  and CIV $\lambda$ 1549. We see evidence for differences: 1) most significantly, stronger ( $EW \sim 5\text{\AA}$ ), NLR emission in the RL sources and 2) a possible excess redshifted BLR (or VBLR) emission in RL sources (this is also present in Figure 7 A–D composite difference of Richards et al. 2002). The former is not a surprise (see e.g. Xu et al. 1999) while the latter, if real, may be an important clue. Since we know that some bin B1 RQ sources also show NLR emission result 1) reflects a lower limit for the mean NLR contribution in Bin B1 RL sources. A comparison shows also that the RL sources from this bin have on average stronger [OIII] and  $H\beta_{NC}$  components (typically by about 30%) than the RQ sources. There is no doubt that RQ sources exist with VBLR components as strong as the strongest observed among the radio-louds (e.g. Sulentic et al. 2000c) so further tests of the red residual are needed.

In order to explore any luminosity correlation with composite spectra we again restrict ourselves to bin B1. Sources were separated into brighter and fainter groups using  $M_V = -25$  as the reference value. This value separates the bin B1 sample into two approximately even

groups. Composite spectra (covering 1000–2000Å) and differences are shown in Fig. 6. One can see a difference in the broad components of all the strongest high ionization lines (Ly $\alpha$ , C IV $\lambda$ 1549, Si IV $\lambda$ 1398 and C III]  $\lambda$ 1909) in the sense that the equivalent width is larger for the lower luminosity composite spectrum (the Baldwin effect? see §4.5 for a thorough discussion). This difference was not seen in the RL vs. RQ comparison. Fainter, lower ionization lines do not show any difference, furthermore they are weak enough that any difference would likely be undetectable.

## 4. Discussion

### 4.1. The Relevance of the Median Composites

The use of composite spectra raises an immediate question. Do median composites yield typical quasar spectra for each bin? For example, is a symmetric profile in a median composite the result of equal numbers of blue and red asymmetric profiles? A visual inspection of our sample spectra shows, e.g. for B-bins, about 60% of sources with a more or less symmetric C IV $\lambda$ 1549 profile, while the remainder show 10, 20 and 10%, respectively red, blue and indeterminate (due to low S/N) asymmetries. This suggests that median composites represent the most typical quasar spectrum and that the changes between our spectral bins are real. If our bin populations had  $\gtrsim 100$  objects then we would use weighted average composites, but medians appear to be a reasonable approach at this time. It is also important to point out that bin sizes were chosen to include sources that are statistically similar within the average parameter measurement errors.

Another important question is whether or not an ensemble of line profiles with a wide distribution of widths, strengths and asymmetries will yield a representative profile of the same type after combination. We see that the many of the lines (especially the strongest) are better fit by a Lorentzian whatever that means physically. Is it possible, for instance, that an ensemble of Gaussian profiles will generate a Lorentzian-like shape in composite spectra or the converse? This might lead to incorrect interpretation, and hence modeling, of line-forming regions. In order to test this possibility we ran a simulation by combining together about 100 artificial line profiles with a wide (normal) distribution of widths and intensities, resembling the real situation to some extent. We performed simulation with both Gaussian and Lorentzian profiles, creating median and average composites from the individual pseudo-spectra. The results suggest that profile type is preserved, i.e. a composite of Gaussians or Lorentzians will preserve their respective profile forms in a composite spectrum.

## 4.2. Inferences From CIV Profile Decomposition

Proper decomposition of emission lines in composite spectra along the E1 sequence offers insights into changes in BLR geometry and kinematics. Several results from this and previous papers provide interesting clues.

Asymmetric blueshifted HIL emission is seen almost exclusively in population A sources. In the most extreme cases a blueshift is also observed in the unusually weak  $[\text{OIII}]\lambda 5007$  features (Zamanov et al. 2002; Marziani et al. 2003c). One simple interpretation that immediately suggests itself involves some kind of outflow from an optically thick emitting region into an optically thin NLR. In a scenario where the broad lines arise from an accretion disk this could involve a high ionization disk outflow or wind. It would be strongest in population A sources and would gradually weaken or even disappear as one proceeds along the E1 sequence toward population B. Along the same sequence an unshifted/symmetric Lorentzian HIL component (which may be analogous to the dominant LIL component) may be growing, in exactly the opposite sense of the blueshifted feature. In fact some theoretical models predict Lorentz-like profile wings (e.g. Penston et al., 1990; Dumont & Collin-Souffrin 1990). The profile may become more Gaussian in the population B region. We have argued in a pre-E1 context that HIL vs. LIL line shifts appeared to be completely uncorrelated for RQ sources and marginally correlated for the RL minority (Marziani et al. 1996). Composite spectra, binned in an E1 context, suggest that CIV and  $\text{H}\beta_{\text{BC}}$  may show analogous emission components except for the blueshifted HIL feature seen only in pop. A that are almost always RQ AGN.

A very broad and redshifted VBLR component is only seen in population B sources and may be present in both HIL and LIL. Since NLR-BLR-VBLR inflections are rarely seen, there may be less spatial/kinematic decoupling between these regions for CIV than is seen for  $\text{H}\beta_{\text{BC}}$ , where clear inflections are common. That is far from proven because we also see LIL profiles with little or no inflection between components. Inflections may be driven by kinematic and/or orientation. There are some indications that the region producing  $\text{CIV}\lambda 1549_{\text{NC}}$  emission is closer to the center than the region producing  $\text{H}\beta_{\text{NC}}$  (Sulentic & Marziani 1999). The  $\text{CIV}\lambda 1549$  VBLR may be most simply interpreted as arising at the inner edge of the classical BLR in analogy to  $\text{H}\beta_{\text{BC}}$  VBLR (Marziani et al. 1993; Sulentic et al. 2000c). The lower redshift of the  $\text{CIV}\lambda 1549$  Pop. B. sources VBLR may also indicate that a high ionization wind is still present in the VLBR since the  $\text{CIV}\lambda 1549$  component is still blueshifted with respect to the corresponding  $\text{H}\beta$  component.

### 4.3. BLR Structure and Kinematics

So far there is no single picture capable of explaining the overall properties of the broad line emitting region. Currently fashionable models involving line emitting clouds near an optically thick accretion disk suffer a number of difficulties. If the motions of the clouds are *Keplerian* then they will collide with the disk and will likely be destroyed on short time scales. If one adopts an outflow/inflow model then the entire profile will show large red or blue-shifts because, the standard optically thick disk will obscure emission from the far side of a flow, while in reality large shifts in line profiles are rare.

Alternatively, emission lines originating from a geometrically thin, optically thick disk (e.g. Dumont & Collin-Souffrin 1990) will show extremely small FWHM when observed face-on. This situation may be relevant for pop. A sources but latest work suggests that the situation is different for RL and, by analogy, other pop. B sources. The most jet-aligned superluminal RL sources, which, should have negligible disk rotation contribution to LIL FWHM, show  $\text{FWHM} \simeq 3000\text{--}4000 \text{ km s}^{-1}$  (Rokaki et al., 2003; Sulentic et al. 2003). It is however true that core-dominated (CD) and superluminal sources with  $i \rightarrow 0^\circ$  show systematically narrower profiles than other (FRII) RL AGN (Sulentic et al. 2003). CD sources are displaced towards lower  $\text{FWHM}(\text{H}\beta_{\text{BC}})$  in the optical E1 plane, which is consistent with orientation predictions. However, even these near pole-on sources lie well above many RQ sources with similar  $R_{\text{FeII}}$ , i.e., they have larger  $\text{FWHM}(\text{H}\beta_{\text{BC}})$  for the same  $R_{\text{FeII}}$  (Sulentic et al. 2003). The results for radio loud sources suggest that we need a considerable velocity dispersion in the vertical direction to account for observed LIL widths ( $\text{FWHM}(\text{H}\beta_{\text{BC}}) \approx 3000 \text{ km s}^{-1}$ ).

The above results might be telling us that the bulk of line emission in RL and Population B RQ sources does not arise from a standard optically thick accretion disk especially when we observe  $\text{FWHM LIL/HIL} \sim 3\text{--}4000 \text{ km s}^{-1}$  in sources reasonably interpreted as almost disk face-on. One candidate for the line emitting region involves the outer self-gravitating part of the disk (Collin & Huré, 2001; Bian & Zhao, 2002). The disk is expected to become gravitationally unstable at some radius  $R_{\text{SG}}$ , where it will break up into rings or discrete self-gravitating clouds. The vertical velocity dispersion of such clouds may be amplified by cloud-cloud encounters. Some studies suggest that the disk can become self-gravitating at a distance from the central black hole as small as 100–200  $R_{\text{G}}$ , where  $R_{\text{G}}$  is the Schwarzschild radius (see for instance Collin & Huré, 2001). A detailed theory for a self-gravitating disks is not yet available, however it is expected that the radius of the self-gravitating region will depend on the central black hole mass and Eddington ratio (and two related and very important parameters: viscosity,  $\alpha$ , and disk opacity). There is no consensus on the correct dependence of  $R_{\text{SG}}$  on parameters like  $M_{\text{BH}}$  or Eddington ratio  $\dot{m} = L/L_{\text{Edd}}$  (here we assume



that the accretion efficiency ( $\eta$ ) does not change with luminosity, otherwise  $\dot{m} = \dot{M}/\dot{M}_{\text{Edd}}$ , where  $\dot{M}_{\text{Edd}} = L_{\text{Edd}}/(\eta c^2)$ .

A very simple approach for exploring this idea involves application of the Toomre stability criterion to a standard Shakura–Sunyaev disk (Shakura & Sunyaev 1973). This will give an estimate of the radius where the stability parameter ( $Q$ ) becomes approximately 1. Different models of the self-gravitating region often predict different  $R_{\text{SG}}$  dependence on the accretion parameters because of different initial assumptions about the outer regions of the disk (i.e. opacity, pressure, etc). Bian & Zhao (2003) obtain in a recent work:  $R_{\text{SG}} \propto \dot{m}^{-0.49} M_{\text{BH}}^{-1.16}$  based on standard accretion disk solutions assuming dominant Kramers opacity. They assume that it is equal to the radius of the BLR  $R_{\text{BLR}}$  (here and below  $R_{\text{SG}}$  is expressed in  $R_{\text{G}}$ ). Collin & Huré (2001) adopt a numerical approach with realistic opacities and get a complex  $R_{\text{SG}}$  dependence roughly approximated by  $R_{\text{SG}} \propto \dot{m}^{0.16} M_{\text{BH}}^{-0.46}$  for the region  $\log(M_{\text{BH}}) = 7 - 9$ ,  $\dot{m} = 0.01 - 1$ . Following these authors, for a BH mass  $M = 10^7 M_{\odot}$  and Eddington ratio  $\simeq 1$ ,  $R_{\text{SG}} \approx 10000 R_{\text{G}}$ , while for  $M = 10^9 M_{\odot}$  and  $\dot{m} \simeq 0.01$ ,  $R_{\text{SG}}$  is less than about  $500 R_{\text{G}}$ .

On the other hand we can consider "superluminal" radio-loud sources with the narrowest RL line profiles:  $\text{FWHM}(\text{H}\beta_{\text{BC}}) \lesssim 3000 \text{ km s}^{-1}$ , and the narrowest Pop. A sources, with  $\text{FWHM}(\text{H}\beta_{\text{BC}}) \lesssim 1000 \text{ km s}^{-1}$ , also likely to be observed at  $i \approx 0^\circ$ . Assuming orbital motion with Keplerian angular velocity ( $\Omega_{\text{K}}$ ), one can write for these apparently face-on sources:

$$\text{FWHM} \simeq \Delta v \simeq \nu \Omega_{\text{K}} R_{\text{SG}} \quad (1)$$

where  $\Delta v$  is the vertical velocity dispersion, assumed to be proportional to the *Keplerian* velocity by a factor of  $\nu$ . A reasonable guess for  $\nu$  is about 0.1–0.2. One can easily show that FWHM of  $3000 \text{ km s}^{-1}$  implies a radius of about  $5000 R_{\text{G}}$  while  $1000 \text{ km s}^{-1}$  implies  $500 R_{\text{G}}$ , values quite close to the size of the self-gravitating region assumed above. Even if the agreement is perhaps fortuitous, and the exact  $R_{\text{SG}}$  dependence is far from certain, it is reasonable to conclude that  $R_{\text{SG}}$  ( $\sim R_{\text{BLR}}$ ) may be smaller in Pop B sources by a factor  $\sim 10$ , and that this may leave a very "small" emitting surface for any standard optically-thick geometrically-thin disk component. Part of the line profile may be produced in the disk if it is illuminated by a geometrically thick inner region or by disk warping (e.g. Bachev, 1999) and if it is not extremely hot (which would completely ionize the lower-ionization species). On the other hand, the presence of a blue-shifted component can be most simply explained as the signature of an outflow from an optically thick disk. The disk-wind scenario can produce blue-shifted high-ionization lines as already suggested in several works (e. g. Murray & Chiang 1997; Bottorff et al. 1997). If our interpretation is correct this implies that the wind strength increases toward the most extreme population A sources (bins A2/A3 with

strongest  $R_{\text{FeII}}$ ). Population B sources may have a much lower, or may not develop, a wind component. Following these considerations we propose a simple BLR scenario (see also Fig. 1 from Collin & Huré, 2001):

- A "hot" innermost accretion region, located inside some transition radius  $R_{\text{Tr}} \lesssim 50 - 100 R_{\text{G}}$ . Our data leave the structure of this region open to speculation, although we may reasonably assume that the continuum region (or part of a geometrically thick, optically thin advection-dominated accretion flow (ADAF; see Narayan, Mahadevan & Quataert 1998 for an exhaustive review) can heat the outer line-emitting region.
- An optically thick, geometrically thin disk whose extent decreases by a factor  $\sim 10$  from Pop. A to Pop B. The heated disk produces a wind that is responsible for the blueshifted  $\text{CIV}\lambda 1549$  component. The outer region of the disk may emit  $\text{H}\beta_{\text{BC}}$  and other LILs as well in Pop. A sources. The disk may become almost negligible in Pop B sources because  $R_{\text{SG}}$  may become as small as  $100 - 200 R_{\text{G}}$  (e.g. Bachev & Strigachev, 2004).
- A self-gravitating and fragmented zone where line emission might arise in dense gas clumps. This region may be the *entire BLR* for Pop. B sources while it may contribute mainly to LIL emission in Pop. A objects.

Within the context of this model + E1 we can eventually explain several observational results from this paper as well as from previous works:

- The different vertical velocity dispersion in the self-gravitating zone for Pop. B (closer) and Pop. A (farther) sources accounts for different line widths at  $i \rightarrow 0^\circ$ ;
- After subtraction of an unshifted/symmetric Lorentzian component the blueshifted residual shows reasonable persistency in shape – the intensity may change but not the overall shape. The blue component becomes marginal at bin A1. This behavior is consistent with the idea that the blue component comes from a disk-generated wind, where the kinematics (velocity field) is strongly affected by the detailed properties (e.g. magnetic field structure and terminal wind velocity). The overall shape of a line arising in a disk wind will be less dependent on the radial distance where the wind originates. In other words, our model provides an easy explanation why population A sources tend to show decoupled HIL–LIL components while Pop. B sources show more similar  $\text{CIV}\lambda 1549$  and  $\text{H}\beta_{\text{BC}}$  profiles. In the most extreme cases, there are sources where the entire  $\text{CIV}\lambda 1549$  profile resembles the blue component alone (e.g. I Zw 1, Ton 28; Sulentic et al. 2000b).

Leighly (2004) presented an interesting explanation of the apparent anticorrelation between the strengths of the central and the blue-shifted (wind) components. The wind that gives rise to the blue-shifted component might filter the EUV ionizing radiation that would otherwise reach the outer, self-gravitating parts (where the unshifted line component might originate). The wind cannot however filter effectively the hard X-rays that are reprocessed in LIL emission in the same region.

An alternative approach is to ascribe the entire profile of CIV in A2/A3 bins to an outflow (wind). In such a case the redward emission is seen either because the disk is (partially) transparent to CIV photons or because of higher inclinations, resulting in significant projection of the Keplerian/radial component of the wind velocity onto the line of sight. Both possibilities seem somewhat unlikely, at least for these extreme bins.

- There are trends between  $\chi$  and FWHM (e.g. Tytler & Fan 1992). Pop. A sources can be explained with a split BLR: inner HIL and an outer LIL emitting regions. Since we expect that gas motion will retain its circular velocity in the wind and will acquire an upward and outward velocity component, the velocity dispersion in the wind will be higher than for a Keplerian velocity component in the disk. LIL emission from the outer, fragmented region will therefore be narrower. In Pop B sources we expect a "normal" BLR stratification: HIL emitted closer to the central continuum source than LIL. In general, we expect that both HIL and LIL will be emitted rather close to the central continuum source, accounting for the rather high ionization spectrum. This outline requires testing with photoionization models.

Reverberation mapping indicates continuum-response times of CIII] $\lambda$ 1909 consistent with the one of H $\beta$ <sub>BC</sub> (at least in NGC 5548; Clavel et al. 1991). This result suggests that CIII] $\lambda$ 1909 is primarily produced in the low-ionization emitting part of the BLR. Under the assumption of nearly constant [Si/C] abundance ratio, the behavior of the Si III] $\lambda$ 1892/CIII] $\lambda$ 1909 intensity ratio along the E1 sequence can then be understood in terms of increasing electron density toward type A3 (M01) in the LIL-emitting BLR. The critical  $n_e$  of the CIII] $\lambda$ 1909 line is  $\sim 10^{9.5} \text{ cm}^{-3}$ , much lower than that of the Si III] $\lambda$ 1892 line,  $\sim 10^{11} \text{ cm}^{-3}$ . Therefore, for  $n_e \gtrsim 10^{10} \text{ cm}^{-3}$ , the CIII] $\lambda$ 1909 line should be more and more collisionally suppressed with increasing  $n_e$ , while the Si III] $\lambda$ 1892 line should become favored. We also observe a consistent increase in the strength of the Al III] $\lambda$ 1860 line, with the intensity ratio Al III] $\lambda$ 1860/CIII] $\lambda$ 1909 reaching  $\sim 0.8$  for spectral type A3 ( $n_e \sim 10^{11} \text{ cm}^{-3}$ ). The Al III] $\lambda$ 1860 line is expected to strengthen with increasing electron density (Baldwin et al. 1996; Korista et al. 1997). However, as pointed out by the referee, chemical abundance may not be constant along the E1 sequence. We do not have information on the

[Si/C] and [Al/C] abundance ratios. Intensity ratios involving nitrogen lines suggests that super-solar metallicity is appropriate for extreme population A (i.e., A3) sources. From Table 2, we have  $Nv\lambda 1240/CIV\lambda 1549 \approx 1$  and  $Nv\lambda 1240/He\ II\lambda 1640 \approx 3$  for A3, while for A1  $Nv\lambda 1240/CIV\lambda 1549 \approx 0.25$ , and  $Nv\lambda 1240/He\ II\lambda 1640 \approx 1.5$ . It is intriguing that we are observing again, for spectral type A3, line ratios that are more frequently found in high- $z$  quasars (Hamann & Ferland 1999). Highly supersolar nitrogen enrichment may have been produced by star formation with a top-loaded initial mass function (Hamann & Ferland 1992; §4.5). It is possible that changes of line ratios from Pop. B to Pop. A and along the A-spectral type are due to *both* an  $n_e$ -increase and a metallicity increase. Quantifying these effects is a challenge for further work.

#### 4.4. Radio Loud Sources: Black Hole Spin *and* Host Morphology?

Comparison of RL and RQ line profiles (§3.2) in the E1 context should begin with a comparison of population A and B sources. The differences that we find between Pop. A and B HIL CIV composites are even larger than for LIL  $H\beta_{BC}$ . We can say with some confidence that sources showing low EW, blueshifted and blue asymmetric  $CIV\lambda 1549$  have low probability ( $P < 1\%$ ) to be radio-loud. Pop.B sources have a reasonably high probability to be RL ( $P \sim 50\%$ ; Marziani et al. 2003b). Since not all pop. B sources are RL we focus (§3.3) on a particular bin (B1) within population B where we can compare  $CIV\lambda 1549$  properties for RQ and RL AGN that appear to be spectroscopically indistinguishable. Our RL-RQ difference spectrum is shown in Figure 5. We see evidence for a significantly stronger NLR component in pop. B RL sources. This might be explained if a significant part of the narrow line emission is produced in interactions between a radio jet and the ambient medium, forming presumably a narrow-line-bright cocoon around the jet (e. g., Steffen et al. 1997; Axon et al. 1998). Aside from a possible excess of redshifted broad line gas in the RL sources, Pop. A RL and RQ line profiles look very similar as was also found for  $H\beta_{BC}$  (Marziani et al. 2003b). The VBLR component, which might be related to this redshifted gas, is seen in both RL and RQ Pop. B AGN (Sulentic et al. 2000c) and, therefore, is not a RL signature. One is tempted to consider host galaxy morphology as a major difference between the RL and RQ sources in bin B1. RL sources tend to be hosted in ellipticals (Pagani et al. 2003) while a typical pop. B RQ source involves a classical Seyfert 1 like NGC 5548, hosted in a spiral. Perhaps the Pop. B emission line spectrum indicates that RL activity is possible as far as physical conditions near the BH are concerned but host morphology dictates whether it happens or not. If it were that simple however we might expect to see many frustrated RL sources involving trapped core emission (unless it is self quenching under that circumstance).

The bin B1 results emphasize the fact that Pop. B RQ and RL sources are spectroscopically indistinguishable as far as *broad* lines are concerned. This may be telling us that radio-loudness is not directly dependent on, or strongly influencing, BLR structure (and therefore – the structure of the accretion disk, at least at  $r \gtrsim 100 R_G$ ). This makes a circumstantial case for the role of black hole spin, which is unlikely to have any influence on the accretion disk structure outside 10–100  $R_G$  where the UV line emission likely originates, at least if the Bardeen-Petterson effect (Bardeen & Petterson, 1975) is not in play. The black hole spin can, however, play a significant role in jet production (e.g. Blandford & Znajek, 1977). The fact that the majority of RL sources occupy B-bins may be associated with a change of the innermost accretion disk structure (from a thin disk to an ADAF?, Różanska & Czerny, 2000, and references therein) that is probably triggered by the lower accretion rate (or by some function of the black hole mass and the accretion rate). If true, the accretion disk structure change (from thin disk to ADAF) will be a necessary but not sufficient condition for radio-loudness (i.e. the ultimate trigger will be the black hole spin, subject to the environmental caveat mentioned above). In this scenario only B-bin objects which contain a rapidly spinning black hole would be able to produce powerful jets.

#### 4.5. A Local "Baldwin Effect" Driven by the Eddington Ratio?<sup>5</sup>

Measurement of broad line EW's reveals both a trend and the lack of a trend (see also §3.1):

- $\text{Ly}\alpha$ ,  $\text{CIV}\lambda 1549$   $\text{MgII}\lambda 2800$  and  $\text{OVI}\lambda 1034$  show a systematic EW decrease by factors of 2 – 4 as one proceeds from bin B1<sup>+</sup> to A3. Table 2 shows the same trend for other lines but caution is needed when interpreting blended lines and data for lines with  $\text{EW} \lesssim 5\text{\AA}$  that have estimated uncertainties  $\gtrsim 30\%$  at the 1- $\sigma$  confidence level.
- The  $\text{NV}\lambda 1240$  line shows no trend with  $\text{EW}(\text{NV}\lambda 1240) \approx 20\text{--}25\text{\AA}$  in all spectral bins.

These results essentially describe the so-called "Baldwin effect" (hereafter BE; originally defined as an anti-correlation between rest frame EW  $\text{CIV}\lambda 1549$  and source luminosity at 1450 $\text{\AA}$ : Baldwin 1977). It is well known that  $\text{NV}\lambda 1240$  does not follow the BE trend (see Sulentic et al. 2000a for references before 1999; Dietrich et al. 2002; Green et al. 2001;

---

<sup>5</sup>We call the  $L/L_{\text{Edd}}$ -dependent Baldwin effect also a "local" Baldwin effect since it is defined through low- $z$ , low to moderate luminosity quasars and Seyfert 1 nuclei, in opposition to the canonical Baldwin effect which emerges considering high- $z$ , high-luminosity quasars

Croom et al. 2002). While the original BE showed a tight correlation involving a few tens of sources, more recent work (Dietrich et al. 2002; Warner et al. 2003) show it to be a very loose correlation that only becomes significant over a wide range in continuum luminosity  $\log(\lambda L_\lambda)=42-48$  ergs  $s^{-1}$  (e.g. Kinney et al. 1990). Considering the large dispersion it is not surprising that several studies using small samples found no evidence for a BE (see Sulentic et al. 2000a for numerical simulations and a thorough discussion of the issue).

The BE-like trend found between our spectral bins does *not* represent a dependence on luminosity. The E1 sequence is independent of source luminosity (Sulentic et al. 2000b) and, is more likely governed by the Eddington ratio (M01; Marziani et al. 2003b). In fact Pop. B spectral bins contain more high luminosity sources than Pop. A because RL in our sample are overluminous, and overrepresented, relative to RQ sources (see also Boroson & Green 1992). Our BE trend is also *not* BH mass-dependent (e.g., Warner et al. 2003): the largest BH masses are again found in population B (M03). If we compare the average  $\dot{m}$  values for our bins (from M03b) with EW(CIV $\lambda$ 1549) measures from our composite spectra we obtain the following approximate relation:  $\log \text{EW}(\text{CIV}\lambda 1549) \simeq 1.35 - 0.67 \log \frac{L}{M}$  excluding bin B1<sup>+</sup>. Our models predict that B1<sup>+</sup> sources are simply more inclined B1 sources (M01). Including B1<sup>+</sup> yields  $\log \text{EW}(\text{CIV}\lambda 1549) \simeq 3.22 - 0.39 \log \frac{L}{M}$  using  $L/M$  bin averages from M03b or  $\log \text{EW}(\text{CIV}\lambda 1549) \simeq 3.54 - 0.47 \log \frac{L}{M}$  if bin averages are taken from this paper ( $L/M$  is measured in Solar units). If we consider all sources (RQ and RL) a robust fitting method yields  $\log \text{EW}(\text{CIV}\lambda 1549) \simeq 3.23 - 0.36 \log \frac{L}{M}$ , which becomes  $\log \text{EW}(\text{CIV}\lambda 1549) \simeq 3.40 - 0.41 \log \frac{L}{M}$  for RQ sources alone.

Parameter dispersion in the Baldwin effect (from  $\text{EW}(\text{CIV}\lambda 1549) \approx 20 - 200 \text{\AA}$ ) is well reproduced by sources spanning the range  $\sim 0.02 - 1$  in  $\dot{m}$  regardless of the fitting solution details. Highest  $\dot{m}$  sources show the lowest EW(CIV $\lambda$ 1549) and it is a well-established fact that NLSy1s show the lowest EW(CIV $\lambda$ 1549) (Marziani et al. 1996; Rogriguez-Pascual et al. 1997; Sulentic et al. 2000a) and are likely to radiate close to the Eddington limit. Many known NLSy1s are relatively low redshift/luminosity sources that tend to blur standard BE correlations at the low luminosity end (see e.g., Brotherton & Francis 1999) because they show EW(CIV $\lambda$ 1549) similar to the high redshift quasars (Sulentic et al. 2000a). Sulentic et al. (2000a) suggested that the BE might be caused by preferential (probably driven by selection effects and/or intrinsic evolution) detection of large  $\dot{m}$  sources at high redshift. In a flux limited sample, where  $L$  and  $z$  are highly correlated, an "evolutionary" (redshift-dependent) Baldwin effect is expected and is indeed found in the Large Bright Quasar Survey (Green et al. 2001). Given a sample that is complete in terms of  $\dot{m}$ , the BE may survive with even larger scatter or disappear depending on the relative importance of evolutionary and selection effects (see Dietrich et al. 2002). Deeper surveys may detect larger EW(CIV $\lambda$ 1549) sources at high redshift: see for example the distribution of EW(CIV $\lambda$ 1549) at  $z \gtrsim 4$  in

Constantin et al. (2002). Intriguingly, they detect several sources with  $\text{EW}(\text{CIV}\lambda 1549) \gtrsim 50 \text{\AA}$  at  $\log L \approx 46.5 \text{ ergs s}^{-1}$ .

Interpretation of the BE has been highly controversial with suggestions encompassing orientation effects (Netzer 1985), selection effects (Sulentic et al. 2000a, and references therein), black hole mass (Wandel 1999; Warner et al. 2003), Eddington ratio (Sulentic et al. 2000a, Shang et al. 2003; Baskin & Laor 2004). A continuum softening with increasing luminosity (Wandel 1999) is a less model-dependent explanation. Warner et al. (2003) suggest that the driving parameter may be the central black hole mass. These authors computed the BH mass using a modified Kaspi et al. (2000) relation, employing FWHM CIV $\lambda 1549$  instead of FWHM H $\beta$  and assuming virial motions. This *does not demonstrate* that mass is driving the BE because it is assumed to be  $M \propto L^{0.7}$ , and this assumption makes the computation in part circular. Furthermore, we question the validity of estimating BH masses using CIV $\lambda 1549$  (e.g. Vestergaard 2002 and Warner et al. 2003; 2004). While H $\beta_{\text{BC}}$  shows average broad line profiles that can be argued to arise in virialized clouds, CIV $\lambda 1549$  is blue asymmetric and blue shifted in about 60% of sources. In many cases the shift is significant and in some – virtually all of the line flux is displaced to the blue side of the local rest frame. It is not at all clear that the clouds (or wind?) producing the HIL emission can be assumed to be virialized. Finally failure to correct for NLR emission in the CIV profile will contribute to the dispersion in BH mass that might be present. NLR emission tends to decrease the dispersion BLR FWHM measures (FWHM measures for pop. B become more like Pop A). Figure 5 shows that NLR uncorrected FWHM CIV measures will underestimate BH mass and overestimate  $L/L_{\text{Edd}}$  values for RL sources.

Our work shows that a CIV $\lambda 1549_{\text{NC}}$  exists in, at least, Pop. B sources and that a significant part (if not all) of CIV $\lambda 1549$  emission in bins A2/A3 arises in a wind. The terminal wind velocity could be only indirectly related to Keplerian (i.e. virialized) motions. The overall velocity dispersion is even less likely to be related to virial motion in near face-on sources, where the accretion disk likely obscures the receding part of the flow. The CIV $\lambda 1549$  line profile in such cases is almost fully blueshifted with respect to the rest frame. While any correlation with mass will be little affected over several orders of magnitude (Warner et al. 2003), any more fundamental correlation with  $\dot{m}$  may be entirely washed out ( $\dot{m}$  range is a factor  $\lesssim 50$ ; Woo & Urry 2002). Comparing FWHM H $\beta$  and CIV in different spectral bins (Pop. B with and without CIV $\lambda 1549_{\text{NC}}$  subtraction) suggests that errors could be at least a factor  $\sim 10$  for some objects (since, for example, the FWHM ratio CIV $\lambda 1549$ H $\beta$  is  $\approx 3$  in IZw1; Marziani et al. 1996; 2003b). However, a shallow trend between EW(CIV $\lambda 1549$ ) and  $L/L_{\text{Edd}}$  is noted in a large sample of quasars of redshift  $0 \lesssim z \lesssim 5$  (Warner et al. 2004), which seems to support our results for  $z \lesssim 0.8$ .

Another circumstantial element supporting a role for the accretion rate  $\dot{m}$  in the BE involves the constancy of  $\text{EW}(\text{Nv}\lambda 1240)$  and the increasing intensity ratio  $\text{Nv}\lambda 1240/\text{Civ}\lambda 1549$  along the sequence from  $\text{B1}^+$  to A3. The large values of  $\text{EW}(\text{Nv}\lambda 1240)$  for all spectral types are suggestive of solar or supersolar metallicity (Turner et al. 2003; Bentz & Osmer 2004). It is not unreasonable to suppose that N may have been enhanced by vigorous formation of massive stars that burn H via the CNO cycle in the AGN circumnuclear regions. The largest enrichment may have occurred in relatively young or rejuvenated quasars radiating at large accretion rates as NLSy1s are thought to be (several NLSy1s hosts may be merging dwarf or barred galaxies; Krongold et al. 2001; Crenshaw et al. 2003).

## 5. Conclusions

We computed and analyzed composite UV spectra for 5 different spectral bins along the main sequence of the E1 optical parameter plane. Data were analyzed following Paper I, which considered similar composite spectra for the optical region involving  $\text{H}\beta$ , our representative LIL. We measured the FWHM and equivalent width of a number of emission lines focussing on  $\text{Civ}\lambda 1549$ , our representative HIL. Our main results include:

- We decompose HIL  $\text{Civ}\lambda 1549$  into possible NLR, BLR and VBLR components many of which have LIL analogs. We consider them to be distinct line emitting regions. Type 2 AGN show only NLR LIL and HIL emission. Type 1 AGN are known with pure BLR, pure VBLR and, most often, composite BLR+VBLR (with and without NLR) spectra if they belong to Population B. A strong asymmetric blueshifted BLR HIL component is unique to population A (bins A2/A3) sources. A reasonably strong and redshifted VBLR is unique to HIL and LIL in population B (bins B1 and  $\text{B1}^+$ ) sources.
- We infer a  $n_e$  trend along the E1 sequence using the ratio of the semi-forbidden lines  $\text{Si III}\lambda 1892$  and  $\text{C III}\lambda 1909$ . Under the assumption of a nearly constant chemical abundance along E1, we find that density increases by about an order of magnitude between bins  $\text{B1}^+$  and A3. However, there are indications that both – density and metallicity may increase from extreme B-bins to extreme A-bins.
- We compare sub-samples of RL and RQ sources in bin B1. We find an excess of NLR and redshifted broad line emission in the RL subsample. The former represents virtual proof that NLR line emission is present in the spectra of many type 1 AGN.
- We advance the following empirically driven model for the structure of the accretion flow:



1. An inner hot optically thin (possibly ADAF) disk, located inside  $R_{\text{Tr}} \lesssim 100 R_{\text{G}}$ .
2. A standard thin disk, between  $R_{\text{Tr}}$  and  $R_{\text{SG}}$ , producing most of the optical continuum. This is the place where a wind may originate and produce the blue-shifted  $\text{CIV}\lambda 1549$  component.
3. An outer self-gravitating region at  $r > R_{\text{SG}}$ , producing most of the broad-line emission.

$R_{\text{Tr}}$  and  $R_{\text{SG}}$  are functions of the accretion parameters. A n eventual discontinuity in their behavior as functions of  $M$  and  $\dot{m}$  may account for the existence of different quasar populations (e.g. Pop. A, B).

- We suggest that the Eddington ratio is the primary driver of the Baldwin effect rather than source luminosity. This suggestion is motivated by the robust BE that we find in E1 which is luminosity independent. This explains why high redshift sources might preferentially show low EW and blueshifted  $\text{CIV}\lambda 1549$  if Pop. A sources are the "seed" (i.e. youngest high accreting lowest mass BH) AGN. This interpretation is supported by comparison of our low redshift sample with first results from higher redshift SDSS quasars. The latter show an increase in the fraction of sources with a blueshifted  $\text{CIV}\lambda 1549$  HIL – a defining characteristic of Pop. A AGN.

RB and JWS acknowledge the kind hospitality and the financial support from the Osservatorio Astronomico di Padova where much of this work has been done. We thank Dr. G. Richards for providing his SDSS composite spectra in an electronic form. We are indebted to an anonymous referee for his/her constructive criticism.

## REFERENCES

- Axon, D. J., Marconi, A., Capetti, A., Maccetto, F. D., Schreier, E., & Robinson, A. 1998, *ApJ*, 496, L75
- Bachev R., 1999, *A&A*, 348, 71
- Bachev R., Strigachev A., 2004, *AN*, 325, No. 4, 1
- Baskin, A. & Laor, A. 2004, *MNRAS*, 350, L31
- Baldwin J. A., 1977, *ApJ*, 214, 679

- Baldwin J. A., Ferland G. J., Korista K. T., et al., 1996, *ApJ*, 461, 664
- Bardeen J.M., Petterson J.A., 1975, *ApJ*, 195, L65
- Bentz M. C., Osmer P. S., 2004, *AJ* 127, 576
- Bian W., Zhao Y., 2002, *A&A*, 395, 465
- Blandford R. D., Znajek R. L., 1977, *MNRAS*, 179, 433
- Bottoff M., Korista K. T., Shlosman I., Blandford R. D., 1997, *ApJ*, 479, 200
- Boroson T.A., Green R.F., 1992, *ApJS*, 80, 109
- Boroson, T. A. 2002, *ApJ*, 565, 78
- Brotherton M. S., Francis P. J., 1999, in "Quasars and Cosmology", ASP Conference Series 162, Eds. G. Ferland and J. Baldwin.
- Clavel, J., et al. 1991, *ApJ*, 366, 64
- Collin S., Huré J.-M., 2001, *A&A*, 372, 50
- Constantin A., Shields J. C., Hamann F., et al., 2002, *ApJ*, 565, 50
- Constantin A., Shields U. C., 2003, *PASP*, 115, 592
- Corbin M. R., Boroson T. A., 1996, *ApJS*, 107, 69
- Corbin, M. R., 1997, *ApJ*, 485, 517
- Crenshaw, D. M., Kraemer, S. B., & Gabel, J. R. 2003, *AJ*, 126, 1690
- Croom S. M., Rhook K., Corbett E. A., et al., 2002, *MNRAS*, 337, 275
- Czerny, B., Nikolajuk, M., Róžańska, A., Dumont, A.-M., Loska, Z., & Zychki, P. T. 2003, *A&A*, 412, 317
- Czerny B., Rozanska A., Kuraszkiwicz J., 2004, *astro-ph/0403507*
- Dietrich, M., Hamann, F., Shields, J. C., Constantin, A., Vestergaard, M., Chaffee, F., Foltz, C. B., & Junkkarinen, V. T. 2002, *ApJ*, 581, 912
- Dumont A. M., Collin-Souffrin S., 1990, *A&A*, 229, 313

- Francis, P. J., Hewett, P. C., Foltz, C. B., Chaffee, F. H., Weymann, R. J., & Morris, S. L. 1991, *ApJ*, 373, 465
- Gammie, C. F., Shapiro, S. L., & McKinney, J. C. 2004, *ApJ*, 602, 312
- Green P. J., Forster K., Kuraszkievicz J, 2001, *ApJ*, 556, 727
- Hamann, F. & Ferland, G. 1992, *ApJ*, 391, L53
- Hamann, F. & Ferland, G. 1999, *ARA&A*, 37, 487
- Horne, K., Peterson, B. M., Collier, S. J., & Netzer, H. 2004, *PASP*, 116, 465
- Jackson N., Browne, I. W. A., 1991, *MNRAS*, 250, 422
- Janiuk, A., Życki, P. T., & Czerny, B. 2000, *MNRAS*, 314, 364
- Kaspi S, Smith P. S., Netzer H., et al., 2000, *ApJ*, 533, 631
- Kellermann K. I., Sramek R., Schmidt M., Shaffer D. B., Green R., 1989, *AJ*, 98, 1195
- Kerber, F., Rosa, M., 2000, *ST-ECF Newsletter No. 27*, 4
- Kinney A. L., Rivolo A. R., Koratkar A. P., 1990, *ApJ*, 357, 338
- Komossa, S., Meerschweinchen, J., 2000, *A&A*, 354, 411
- Korista K., Baldwin J., Ferland G., Verner D., 1997, *ApJS*, 108, 401
- Korista K. T., Goad M. R., 2004, *ApJ*, 606, 749
- Krongold Y., Dultzin-Hacyan D., Marziani P., 2001, *AJ*, 121, 702
- Kuraszkievicz, J. K., Green, P. J., Crenshaw, D. M., Dunn, J., Forster, K., Vestergaard, M., & Aldcroft, T. L. 2004, *ApJS*, 150, 165
- Leighly K., 2004, *astro-ph/0402452*
- Maccarone, T. J., Gallo, E., & Fender, R. 2003, *MNRAS*, 345, L19
- Marziani P., Sulentic J. W., Calvani M., Perez E., Moles M., Penston M. V., 1993, *ApJ*, 410, 56
- Marziani, P., Sulentic, J. W., Dultzin-Hacyan, D., Calvani, M., Moles, M., 1996, *ApJS*, 104, 37

- Marziani P., Sulentic J.W., Zwitter T., Dultzin-Hacyan D., Calvani M., 2001, *ApJ*, 558, 553 (M01)
- Marziani P., Sulentic J. W., Zamanov R., Calvani M., Dultzin-Hacyan D., Bachev R., Zwitter T., 2003a, *ApJS*, 145, 199 (M03)
- Marziani P., Zamanov R., Sulentic J. W., Calvani M., 2003b, *MNRAS*, 345, 1133
- Marziani, P., Zamanov, R., Sulentic, J. W., Calvani, M., & Dultzin-Hacyan, D. 2003c, *Memorie della Societa Astronomica Italiana*, 74, 492
- Mathur, S., 2000, *MNRAS*, 314, L17
- Mirabel, I. F. 2004, *ArXiv Astrophysics e-prints*, astro-ph/0404156
- Murray N., Chiang J., 1997, *ApJ*, 474, 91
- Narayan, R., Mahadevan, R., & Quataert, E. 1998, *Theory of Black Hole Accretion Disks*, edited by Marek A. Abramowicz, Gunnlaugur Bjornsson, and James E. Pringle. Cambridge University Press, 148
- Netzer H., 1985, *MNRAS*, 216, 63
- Nicastro, F. 2000, *ApJ*, 530, L65
- Pagani, C., Falomo, R., & Treves, A. 2003, *ApJ*, 596, 830
- Penston M. V., Croft S., Basu D., Fuller N., 1990, *MNRAS*, 244, 357
- Peterson, B. M. 1993, *PASP*, 105, 247
- Peterson, B. M., 1997, *An introduction to active galactic nuclei*, Cambridge U Press
- Pounds, K. A., Done, C., & Osborne, J. P. 1995, *MNRAS*, 277, L5
- Richards G. T., Vanden Berk D. E., Reichard T. A., Hall P. B., Schneider D. P., SubbaRao M., Thakar A. R., York D. G., 2002, *AJ*, 124, 1
- Rodriguez-Pascual P. M., Mas-Hesse J. M., Santos-Lleo M., 1997, *A&A*, 327, 72
- Rokaki E., Lawrence A., Economou F., Mastichiadis A., 2003, *MNRAS*, 340, 1298
- Różanska A., Czerny B., 2000, *A&A*, 360, 117
- Schlegel D. J., Finkbeiner D. P., Davis M., 1998, *ApJ*, 500, 525

- Schneider, D. P., et al. 2002, *AJ*, 123, 567
- Shakura N. I., Sunyaev R. A., 1973, *A&A*, 24, 337
- Shang, Z., Wills, B. J., Robinson, E. L., Wills, D., Laor, A., Xie, B., & Yuan, J. 2003, *ApJ*, 586, 52
- Snedden S. A., Gaskell, C. M., 2004, astro-ph/0403174
- Steffen, W., Gomez, J. L., Raga, A. C., & Williams, R. J. R. 1997, *ApJ*, 491, L73
- Sulentic, J. W., Marziani, P., 1999, *ApJ*, 518, L9
- Sulentic, J. W., Calvani, M., & Marziani, P. 2001, *The Messenger*, 104, 25
- Sulentic J.W., Marziani P., Dultzin-Hacyan D., 2000a, *AR A&A*, 38, 521
- Sulentic J. W., Zwitter T., Marziani P., Dultzin-Hacyan D., 2000b, *ApJ*, 536, L5.
- Sulentic J. W., Marziani P., Zwitter T., Dultzin-Hacyan D., Calvani M. 2000c, *ApJ*, 545, L15
- Sulentic J. W., Marziani P., Zamanov R., Bachev R., Calvani M., Dultzin-Hacyan D., 2002, *ApJ*, 566, L71 (Paper I)
- Sulentic, J. W., Stirpe, G. M., Marziani, P., Zamanov, R., Calvani, M., & Braitto, V. 2004, *ArXiv Astrophysics e-prints*, astro-ph/0405279
- Sulentic J. W., Zamfir S., Marziani P., Bachev R., Calvani M., Dultzin-Hacyan D., 2003, *ApJ*, 597, L17
- Turner T. J., Kraemer S. B., Mushotzky R. F., et al., 2003, *ApJ*, 594, 128
- Tytler D., Fan X-M, 1992, *ApJS*, 79, 1
- Vanden Berk, D. E., et al. 2001, *AJ*, 122, 549
- Véron-Cetty, M.-P., Véron, P. 2001, *A&A*, 374, 92 (VCV01)
- Véron-Cetty M.-P., Véron P., Goncalves A. C., 2001, *A&A*, 372, 730
- Wandel A., 1999, *ApJ*, 527, 649
- Warner C., Hamann F., Dietrich M., 2003, *ApJ*, 596, 72
- Wills B. J., Thompson K. L., Han M., et al., 1995, *ApJ*, 447, 139

Woo J.-H., Urry C. M., 2002, *ApJ*, 579, 530

Xu C., Livio M., Baum S., 1999, *AJ*, 118, 1169

Zamanov R., & Marziani P., 2002, *ApJ*, 571, L77

Zamanov R., Marziani P., Sulentic J. W., Calvani M., Dultzin-Hacyan D., Bachev R., 2002, *ApJ*, 567, L9

Table 1. DEFINITION OF SPECTRAL TYPES

Bin (1)	FWHM( $H\beta_{BC}$ ) (2)	$R_{FeII}$ (3)	$N_{tot}$ ( $N_{RL}$ ) (4)	S/N (5)	$\langle M_V \rangle$ ( $\sigma$ ) (6)	$\langle z \rangle$ ( $\sigma$ ) (7)	EW([OIII]) (8)	EW( $H\beta$ ) (9)
A3	<4000	>1.0	10 (2)	39	-23.1 (2.1)	0.20 (0.20)	20 (5)*	50 (54)
A2	<4000	0.5 - 1.0	14 (1)	35	-24.4 (1.6)	0.26 (0.22)	18 (9)	67 (63)
A1	<4000	<0.5	40 (12)	74	-24.3 (2.2)	0.26 (0.24)	44 (25)	95 (89)
B1	4000 - 8000	<0.5	54 (28)	87	-25.1 (1.7)	0.36 (0.24)	46 (26)	98 (95)
B1 <sup>+</sup>	>8000	<0.5	21 (17)	52	-25.4 (1.4)	0.44 (0.22)	60 (34)	99 (98)

\*We provide the median values (in brackets) for the last two columns as well. Due to significantly dispersed EW distributions and the small number of objects in some bins, the medians may differ significantly from the averages, especially for [OIII].

Table 2. LINE MEASUREMENTS

Line Id.	A3		A2		A1		B1		B1 <sup>+</sup>	
	EW ( $\sigma$ )	FWHM ( $\sigma$ )	EW ( $\sigma$ )	FWHM ( $\sigma$ )	EW ( $\sigma$ )	FWHM ( $\sigma$ )	EW ( $\sigma$ )	FWHM ( $\sigma$ )	EW ( $\sigma$ )	FWHM ( $\sigma$ )
OVI 1034	-	-	-	-	17 (4)	3770 (500)	21 (6)	4350 (600)	18 (4)	5510 (700)
CIII 1176	-	-	4 (3)	3600 (2000)	1 (1)	5100 (2000)	4 (3)	5350 (2500)	-	-
Ly $\alpha$ 1216	48 (15)	2960 (700)	92 (21)	2960 (500)	101(25)	3450 (500)	116(21)	3700 (400)	93 (18)	5420 (400)
NV 1240	26 (9)	3870 (700)	21 (7)	4110 (700)	17 (6)	3380 (600)	28 (9)	5080 (800)	25 (6)	7250 (900)
SiII 1264	3 (2)	2250 (1000)	2 (1)	1420 (800)	-	-	-	-	-	-
SiII 1306	6 (2)	3530 (500)	5 (1)	2290 (300)	3 (1)	2290 (300)	4 (1)	3670 (500)	3 (1)	4820 (1000)
CII 1335	2 (1)	1970 (500)	3 (1)	1680 (300)	1 (1)	2240 (300)	1 (1)	2240 (600)	1 (1)	3590 (1500)
SiIV 1398	16 (3)	4500 (400)	16 (3)	3860 (400)	13 (3)	4070 (400)	11 (2)	3640 (400)	12 (2)	6000 (400)
NIV] 1486	-	-	-	-	2 (1)	2610 (800)	1 (1)	3020 (800)	-	-
CIV 1549	23 (4)	4160 (400)	35 (9)	3290 (400)	69 (16)	3480 (400)	83 (16)	4260 (400)	79 (10)	6190 (400)
HeII 1640	8 (2)	5850 (700)	10 (2)	4750 (500)	11 (2)	4570 (400)	11 (2)	4930 (500)	4 (1)	4750 (600)
OIII] 1663	2 (1)	2880 (800)	5 (2)	4140 (700)	4 (1)	3060 (500)	7 (2)	4320 (700)	5 (2)	3600 (700)
NIII] 1750	4 (3)	2050 (1000)	-	-	-	-	4 (3)	4410 (1500)	-	-
AlIII 1860	8 (4)	4670 (1200)	5 (3)	3860 (1200)	2 (1)	4180 (1000)	3 (2)	4700 (2000)	3 (2)	5700 (2500)
SiIII] 1892	7 (3)	1900 (800)	8 (2)	1740 (700)	6 (2)	2530 (600)	5 (3)	2530 (1000)	3 (2)	3010 (1500)
CIII] 1909	10 (4)	2350 (800)	15 (4)	1720 (700)	17 (4)	2510 (500)	20 (7)	3140 (700)	18 (9)	3920 (1200)
MgII 2798	12 (8)	2030 (700)	14 (4)	1500 (700)	16 (2)	1600 (600)	40 (8)	3960 (600)	44 (8)	6540 (600)
FeIIUV	22 (10)	3000 (-)	16 (8)	3000 (-)	9 (5)	3000 (-)	7 (5)	5000 (-)	7 (5)	9000 (-)



Table 3. CIV $\lambda$ 1549 COMPONENTS

S.T.	Component 1				Component 2			
	Type	$\lambda$	FWHM	Strength (%)	Type	$\lambda$	FWHM	Strength (%)
A3	Lor	1547.3	2220	50	Blue	1532	4800	50
A2	Lor	1547.8	2600	76	Blue	1534	3900	24
A1	Lor	1547.7	3580	100	-			
B1	Gau	1548.3	4170	42	Gau	1555.8	15590	58
B1 <sup>+</sup>	Gau	1547.8	4780	28	Gau	1552.6	17480	72

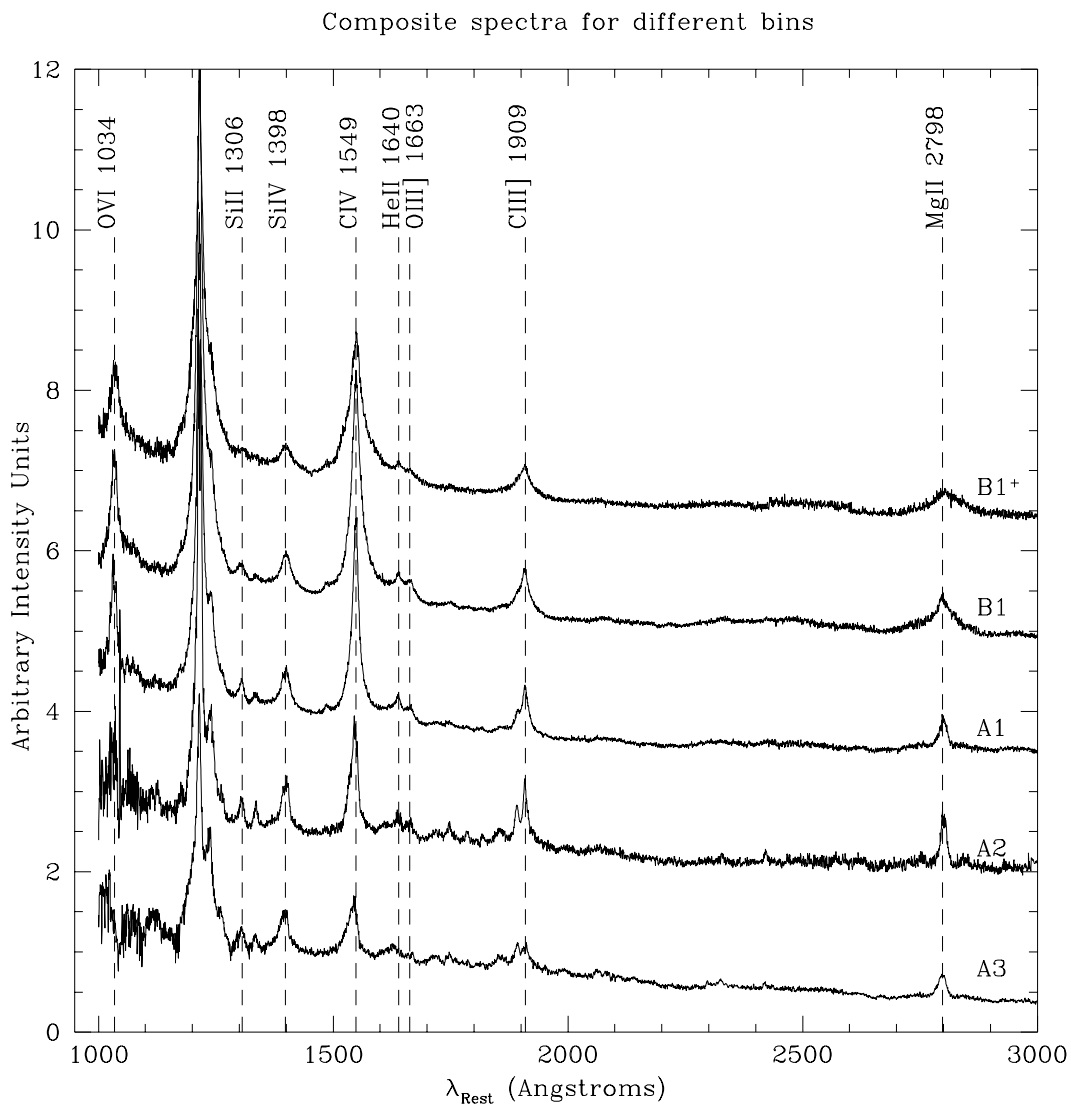


Fig. 1.— Median HST spectra for the 5 spectral types considered in this paper, with identification of the strongest emission lines. Each spectrum was corrected for the interstellar extinction and shifted to the rest frame before being processed. Horizontal scale is rest frame wavelength in Ångstroms, vertical scale is in arbitrary  $F_{\lambda}$  intensity units. Spectra have been offset on the vertical axis for clarity.

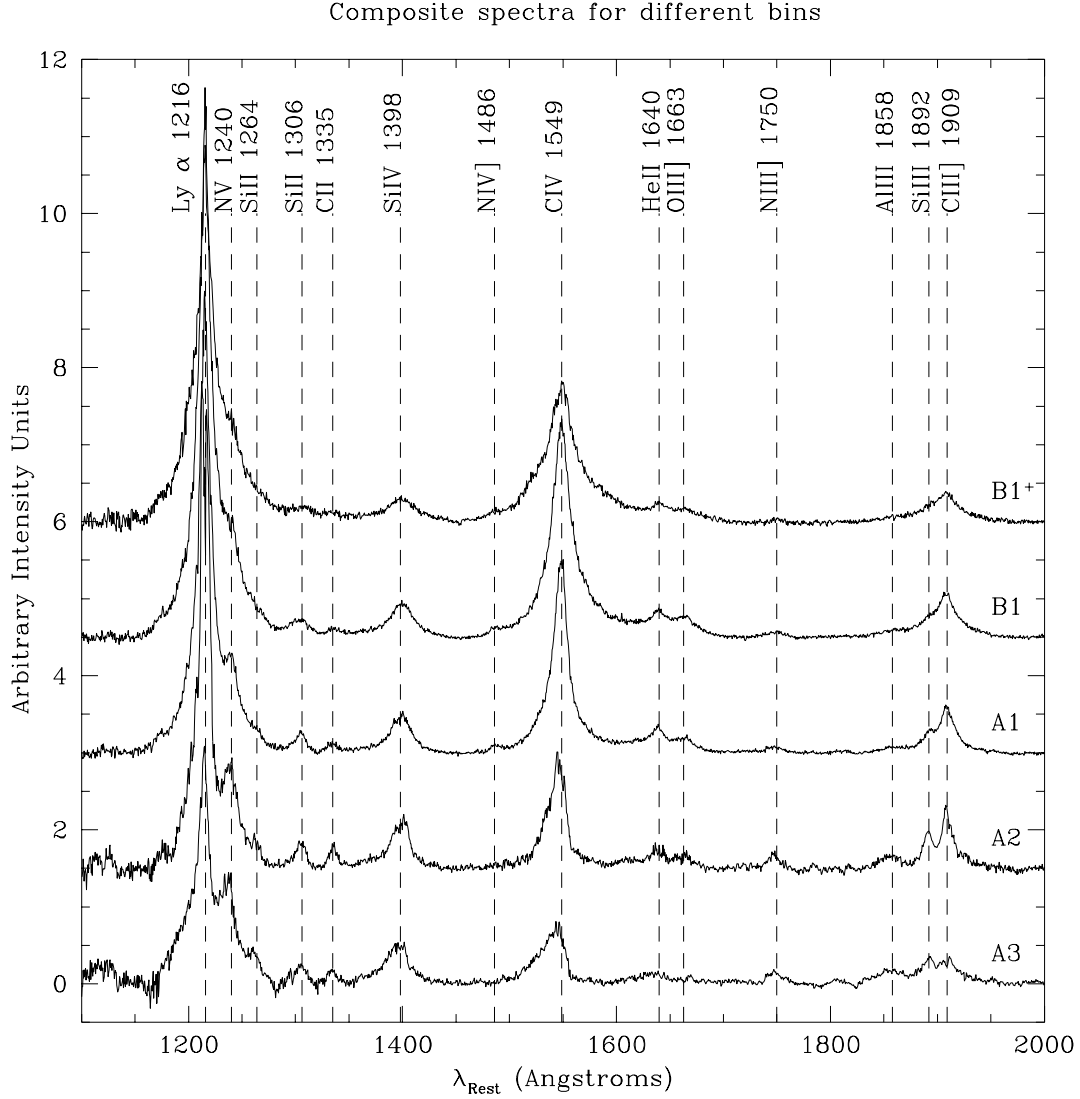


Fig. 2.— The rest frame region of the median spectra between  $1150 \text{ \AA}$  and  $1950 \text{ \AA}$  is shown after continuum and  $\text{FeII}_{\text{UV}}$  emission subtraction. As for Fig. 1, spectra have been offset for clarity. All lines for which we report equivalent width and FWHM in Table 2 are identified. Horizontal scale is rest frame wavelength in  $\text{\AA}$ .

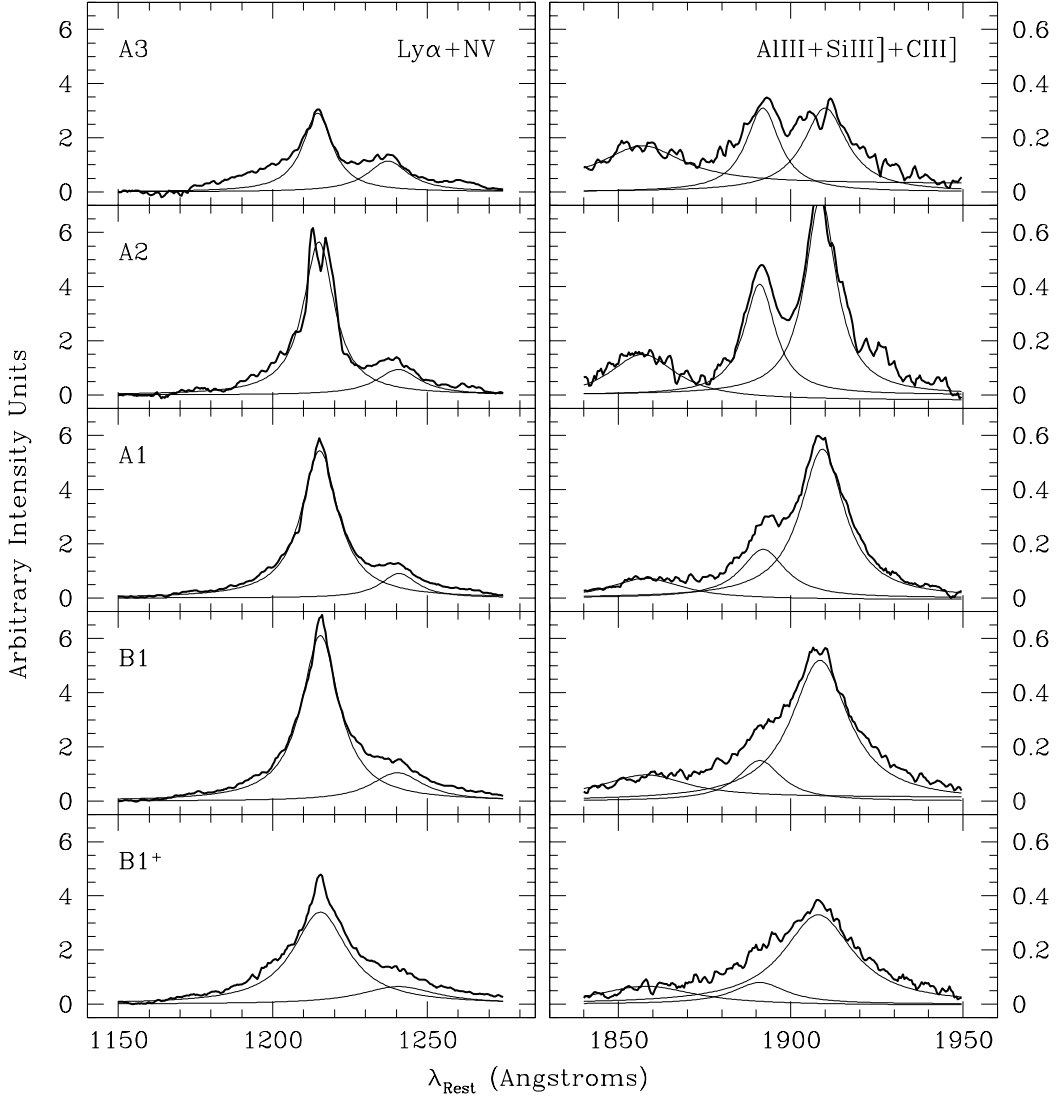


Fig. 3.— Decomposition of blended lines for the spectral types considered in this paper. Left panels: Ly $\alpha$  + NV $\lambda$ 1240; right panels Al III $\lambda$ 1860, Si III $\lambda$ 1892 and C III $\lambda$ 1909. To all blends we subtracted in advance the underlying continuum and an Fe II<sub>UV</sub> emission template; Fe II<sub>UV</sub> emission is however weak around Ly $\alpha$  and C III $\lambda$ 1909. Thick lines show the profiles we fit; thin lines show individual line contributions (assumed to have Lorentzian profiles) to the blend. No narrow component is subtracted prior to the fitting in any of the lines. While the NV $\lambda$ 1240 equivalent width remains approximately constant, the Si III $\lambda$ 1892/ C III $\lambda$ 1909 intensity ratio decreases monotonically along the sequence of spectral types. Horizontal scale is rest frame wavelength in Å; vertical scale is intensity in arbitrary units.

CIV 1549 profiles for different bins

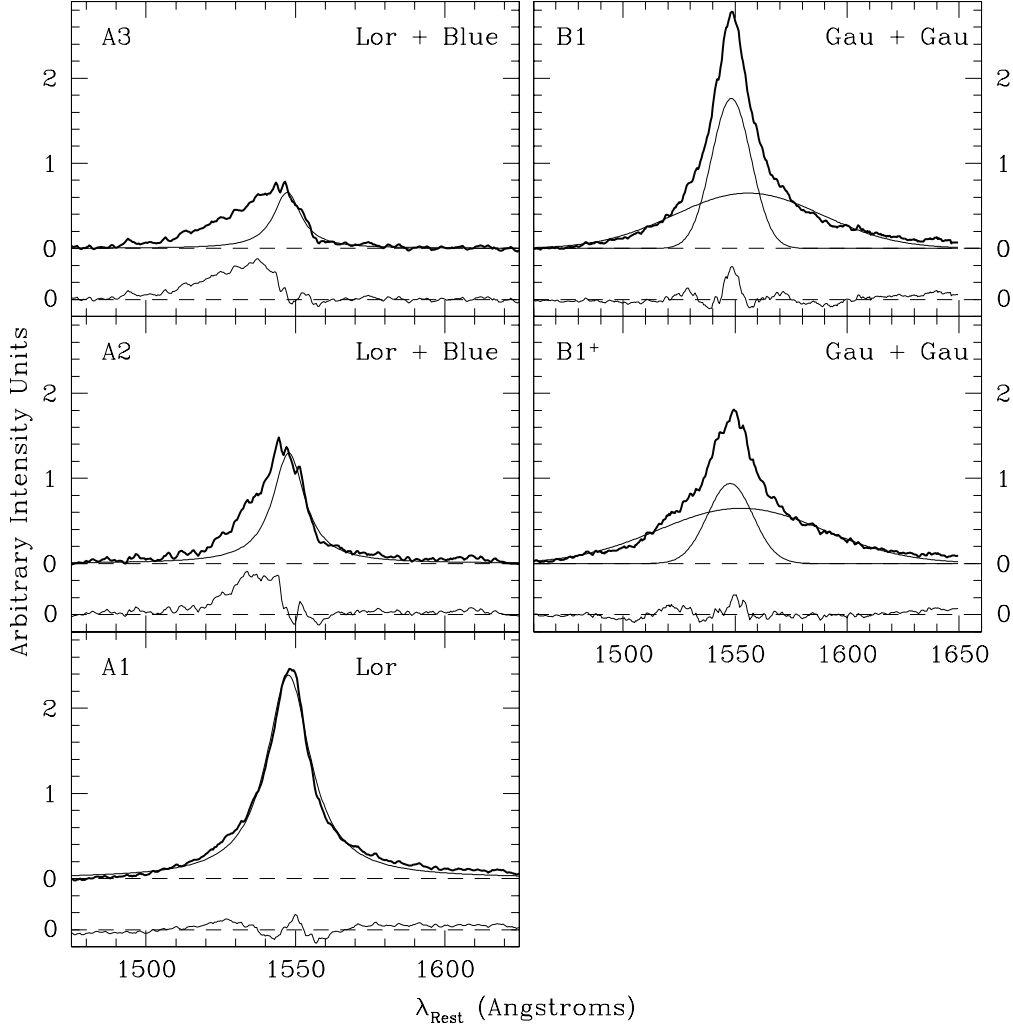


Fig. 4.— CIV $\lambda$ 1549 line profile decomposition for the spectral types considered in this paper. The fitted data are shown by thick lines; they are obtained from the continuum and FeII<sub>UV</sub> subtracted spectra after He II $\lambda$ 1640 and OIII $\lambda$ 1663 and NIV $\lambda$ 1486 removal. For bin A3 and A2, the thin line superimposed to the data shows the best fit provided by an unshifted Lorentzian line to the CIV $\lambda$ 1549 red wing. The residual is a broad and blueshifted feature, possibly associated with outflows. For bin A1, a symmetric Lorentzian provides a satisfactory fit. For spectral types B1 and B1+, two Gaussian profiles, similar to the one used by Sulentic et al. in Paper I to fit H $\beta$ <sub>BC</sub> provide a satisfactory fits to the CIV $\lambda$ 1549 broad component. Narrow central residuals seen in A1 and B-bins can possibly be associated with the contribution of the NLR.

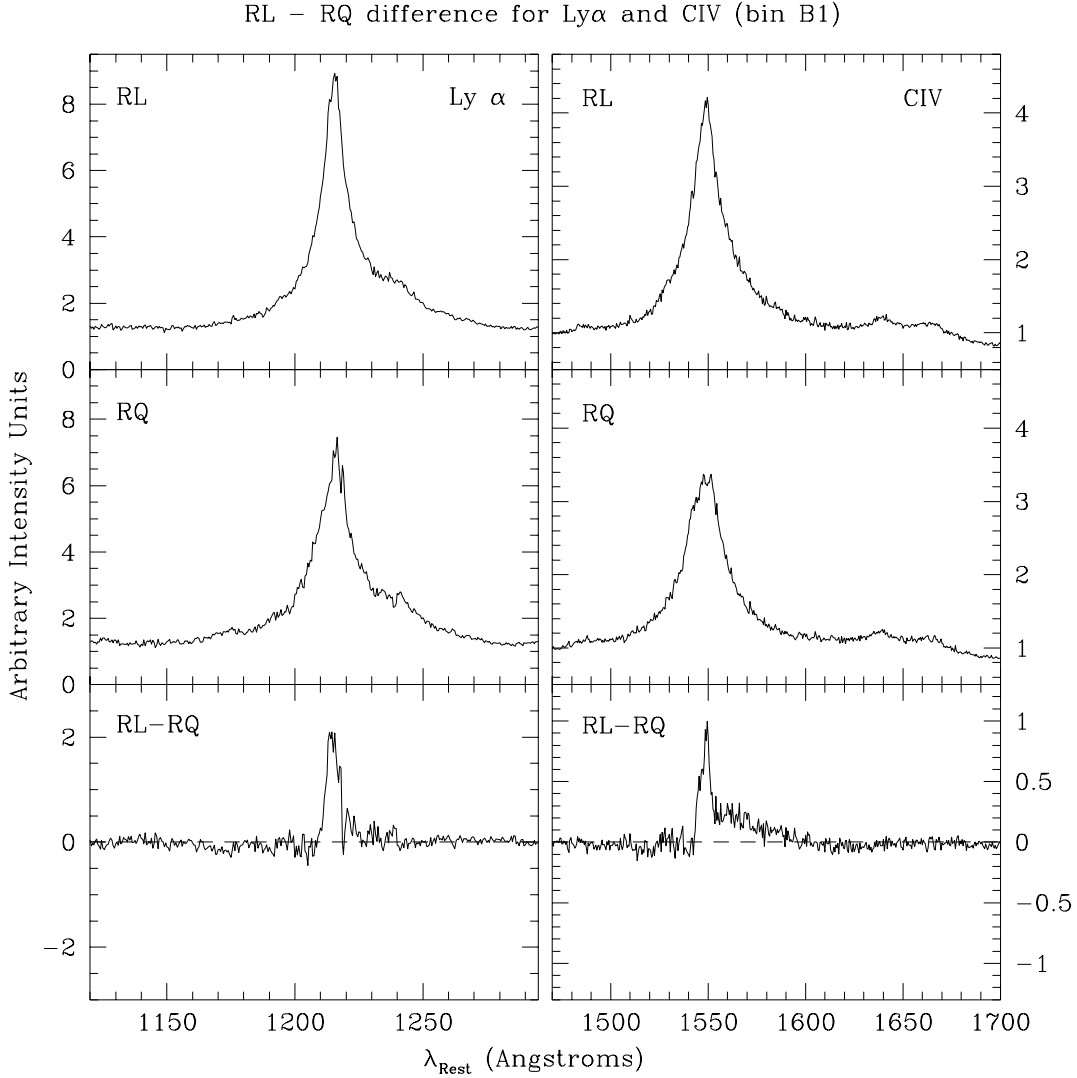


Fig. 5.— Ly $\alpha$  (left panels) and CIV $\lambda$ 1549 profiles (right) for radio-loud (top panels) and radio-quiet (middle panels) quasars. Note that, unlike in Fig. 3, contaminating lines have not been removed. Residuals (bottom panels) show that the main difference is due to a stronger narrow component in radio-loud sources. Horizontal scale is rest frame wavelength in Ångstroms; vertical scale is in arbitrary intensity units.

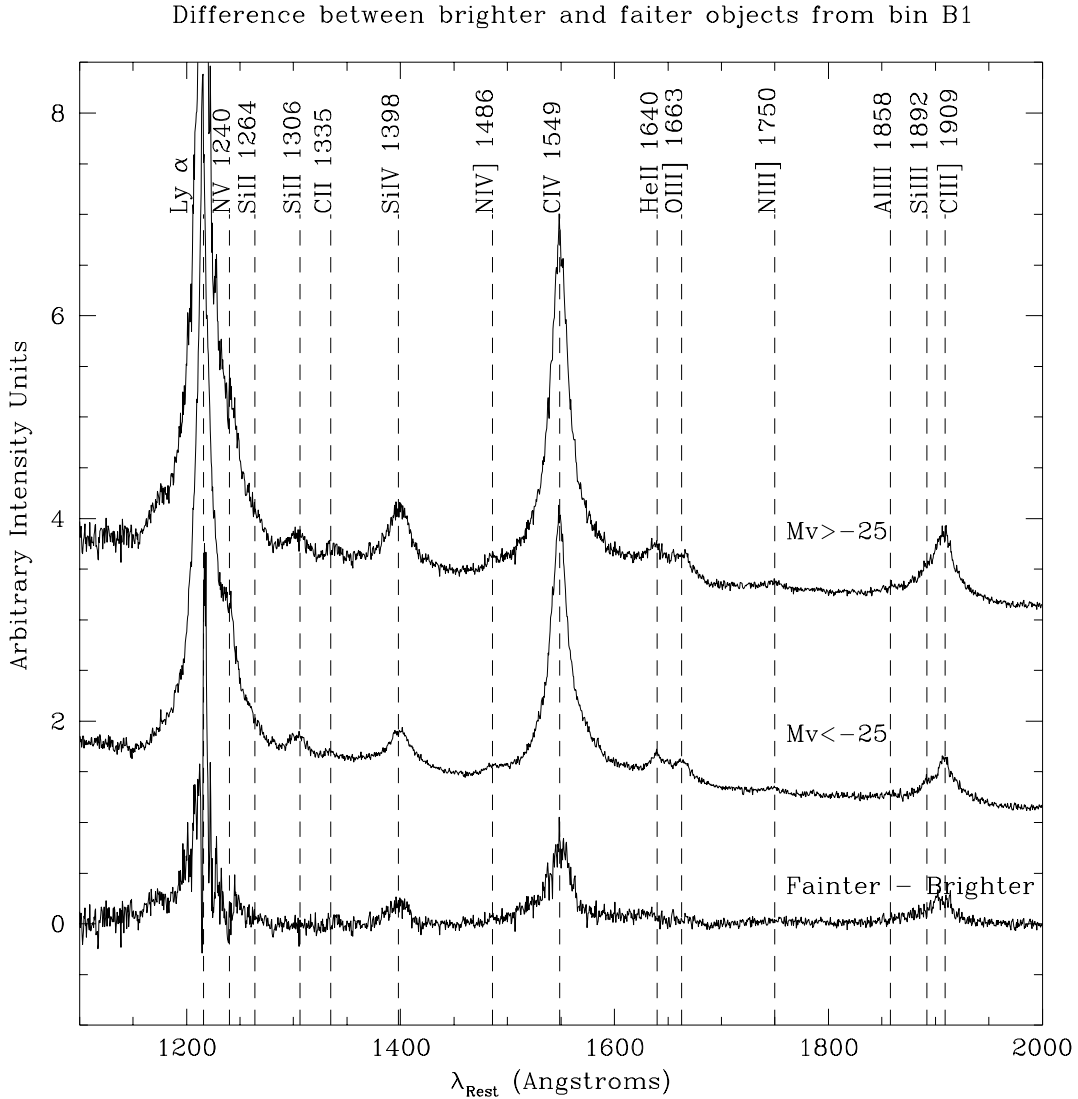


Fig. 6.— Similar division as the one shown in Fig. 5 is presented here – this time we show the difference between the fainter objects and the brighter objects from bin B1. The separation value of the absolute V-band luminosity  $M_V = -25$  is chosen in order to create two equally represented groups. The Baldwin effect (anticorrelation of the equivalent width of a line with the luminosity is apparent for lines like  $Ly\alpha$ ,  $Si\ IV\lambda 1398$ ,  $CIV\lambda 1549$ ,  $Si\ III]\lambda 1892$ , but not for lines like  $NV\lambda 1240$  and  $Si\ II]\lambda 1306$ . The situation is unclear for  $He\ II\lambda 1640$ ,  $OIII]\lambda 1663$  and other lines due to their lower contrast.